




Article

Photocatalytic Performance of Functionalized Biopolymer for Neodymium (III) Sorption and the Recovery from Leachate Solution

Mohammed F. Hamza ^{1,2,*} , Hamed Mira ², Mahmoud S. Khalafalla ², Ji Wang ^{1,*}, Yuezhou Wei ^{1,3} , Xiangbiao Yin ¹, Shunyan Ning ¹ , Khalid Althumayri ⁴ and Amr Fouda ⁵ 

¹ School of Nuclear Science and Technology, University of South China, Hengyang 421001, China

² Nuclear Materials Authority, P.O. Box 530, El-Maadi, Cairo 11728, Egypt

³ School of Nuclear Science and Engineering, Shanghai Jiao Tong University, Shanghai 200240, China

⁴ Department of Chemistry, College of Science, Taibah University, Al-Madinah Al-Munawarah 30002, Saudi Arabia

⁵ Botany and Microbiology Department, Faculty of Science, Al-Azhar University, Nasr City, Cairo 11884, Egypt

* Correspondence: m_fouda21@usc.edu.cn (M.F.H.); wangji@usc.edu.cn (J.W.); Tel.: +20-111-668-1228 (M.F.H.); +86-734-828-2251 (J.W.)

Abstract: Successive grafting of new sorbent bearing amino phosphonic groups based on chitosan nano magnetite particles was performed through successive coupling with formaldehyde. The produced composite was characterized by the high sorption capacity toward rare earth elements (REEs) and consists of different types of functional groups (phosphonic, hydroxyls and amine groups) that are used for enhancing the sorption properties. The chemical modification and the sorption mechanism were investigated through different analytical tools; i.e., FTIR, SEM, SEM-EDX, TGA, BET (surface area) and pH_{pzc} . The sorption was investigated toward Nd(III) as one of the REE(III) members under ultraviolet (UV) and visible light (VL) conditions. The optimum sorption was found at pH_0 4 and the sorption capacity was recorded at 0.871 and 0.779 mmol Nd g⁻¹ under UV and VL respectively. Sorption isotherms and uptake kinetics were fitted by Langmuir and Sips and by pseudo-first order rate equation (PFORE) for the functionalized sorbent, respectively. The sorbent showed a relatively high-speed sorption kinetic (20 min). The bounded metal ions were progressively eluted using 0.2 M HCl solution with a desorption rate 10–15 min, while the loss in the total capacity after a series of sorption recycling (sorption/desorption) (five cycles) was limited (around 3%) with 100% of the desorption efficiency, indicating the high stability of the sorbent toward an acidic medium. The sorbent was used for the recovery of REEs from leach liquor residue after pretreatment for the extraction of particular elements. From these results (high loading capacity, high selectivity and high stability against acid treatments), we can see that the sorbent is a promising tool for the selective recovery of rare earth elements in the field of metal valorization.

Keywords: phosphorylated sorbent; photocatalysis; chitosan; rare earth elements; neodymium ions; metal desorption



Citation: Hamza, M.F.; Mira, H.; Khalafalla, M.S.; Wang, J.; Wei, Y.; Yin, X.; Ning, S.; Althumayri, K.; Fouda, A. Photocatalytic Performance of Functionalized Biopolymer for Neodymium (III) Sorption and the Recovery from Leachate Solution. *Catalysts* **2023**, *13*, 672. <https://doi.org/10.3390/catal13040672>

Academic Editor: Mohd Rafatullah

Received: 9 February 2023

Revised: 27 March 2023

Accepted: 28 March 2023

Published: 30 March 2023



Copyright: © 2023 by the authors. Licensee MDPI, Basel, Switzerland. This article is an open access article distributed under the terms and conditions of the Creative Commons Attribution (CC BY) license (<https://creativecommons.org/licenses/by/4.0/>).

1. Introduction

Rare-earth elements (REEs) consist of seventeen members that, with the exception of yttrium and scandium, range in atomic number from 57 (lanthanum) to 71 (lutetium). They are all with many similar properties [1,2] and are thus referred to as “lanthanides”. Because of their unusual physical and chemical properties, they are used in different varieties of industrial and technological applications [3,4]. The need for rare earth elements (REEs) has increased, because of their widespread use in high-tech applications [5] and advanced technologies; as a kind of valuable additive (composite) for automotive catalytic converters, the military, and green technologies; and in mobile phones, televisions, light-emitting diodes, and computer hard disks [6,7]. Some REEs(III) (i.e., Dy, Er) have been used for

applications in the nuclear industry, for example in the control rods that regulate nuclear reactors, in shielding materials, and for the quantifying ionizing of radiation [8]. Therefore, the development of more performant separation procedures for REEs has become necessary, especially given that it is limited to a small number of countries [9]. Many policies have been established to promote the development of REE production from geological tailing materials and industrial byproducts [10–15]. Other successful method have been performed that use unconventional techniques such as production from red mud tailing material [16,17] or phosphogypsum and phosphoric acid production units [18–24], fly ash, coal fines, mining tailings, phosphorus-based products and permanent magnets [25–27]. Relatively purified REEs have been obtained using a physical separation, followed by a leaching and then selective extraction, with this method being used effectively for the recovery of REEs. Other methods have been used to decrease the environmental impacts (reduce pollution) [28].

The extraction of REEs from leaching solution is generally accomplished by a variety of conventional methods, including chemical precipitation [29,30] and solvent extraction [31], which are mainly used for the extraction of high concentrated metal ions in solutions. Ion exchange methods [32–35], impregnated resins [36–38] and chelating composites [39–44] are used as tools for the efficient extraction of these elements in less concentrated solutions. Solid phase extraction (SPE) is based on the association between organic ligands and REEs. Other tools pay specific attention to the extraction of metal ions and heavy elements such as carbon [45,46], graphene-based sorbents [47], silica functionalized composite [48–50], clays [51,52], NbCo-MOF [53] and functionalized biopolymers [54,55].

Biosorbents and biopolymers are easily functionalized (due to their hydrophilic properties) by substitute/grafting reactive groups in order to increase the uptake capacity of the sorbent for metal ions. This improves sorption kinetics, facilitates more efficient recovery, and improves other physico-chemical properties. The presence of amine, carboxylic and hydroxyl groups in the structure of these biopolymers (for example chitosan, gums and alginate) facilitates such chemical modification. Among the groups for which grafting improves sorption capacity are sulfonic acid [56], amidoxime [57], amino acids [54,58], heterocyclic groups [59–61], phosphorus groups [62,63] quaternary ammonium groups [64–67], amino-sulfonic acid [68], amine and thion [69], and green synthesized materials [70].

Chitosan is considered one of the most abundant biopolymers and is known as an excellent biosorbent of heavy metal ions, dyes and proteins from various media due to their low cost and their high amino and hydroxyl group contents. Chitosan can be modified easily by chemical or physical processes (acquired by grafting new functional groups) or to condition polymers as membranes, fibers, hollow fibers, and gel beads [71]. It has a singular property, through the known polysaccharides and because of its cationic behavior, that allows it to be dissolved, modified and shaped by protonated amines. This means it can improving sorption kinetics and solid liquid separation by reducing its size, through its coating on magnetite and other nanoparticles, in order to produce nano/micro structured composites. The presence of amines and hydroxyls on their structure allow for chemical modification [72] and the recovery of metal ions and complexes. Several grafting groups have been created, including carboxylic group derivatives [73,74], poly(amines) [75,76], and amino-phosphonic [77,78] and phosphonic [79] moieties. These improve the selectivity of chitosan derivatives towards phosphate ions by immobilizing nano-sized $\text{La}(\text{OH})_3$ [80].

A new process of phosphorylating on chitosan particles has been achieved, one which produces a very efficient sorbent for the recovery of rare earth elements and for which the highest sorption capacities were performed in a mild acid solution. In this work the neodymium element (as an REE with essential uses in many industries, including the automobile industry and in permanent magnets, lasers, cryo-coolers, and high-tech glasses) was tested to evaluate the synthesized sorbents (under UV and VL conditions) before application in REE recovery in pregnant raffinate solution (produced from the acidic leaching of the residual by-product).

A deep characterization of the synthesized material in terms of its structural and textural properties and the binding mechanisms toward metal ions has been discussed in

the above, first part of the manuscript. This was performed through a wide diversity of analytical tools, including SEM-EDX, TEM, FTIR, elemental analysis (EA), TGA, pH_{pzc} and surface area (nitrogen sorption desorption properties). The second part of this work, concerning study of the sorption properties and the sorption capacity toward neodymium metal ion through the effects of pH, uptake kinetics, isotherm experiments, selectivity tests (from equimolar solution of different metal ions, expected to be associated with neodymium in the leaching liquor), metal desorption, and sorbent recycling. This part was performed three times for reproducibility under visible light (VL) and under UV emission and is represented in the figures as curves with a standard deviation obtained through the application of error bars. The final part of this work studies the evaluation of the sorbent's ability to recover rare earth elements from the pregnant leach liquor (polymetallic solution) that is derived from the acidic leaching of ore residue. From loading experiments, we observed a specific selectivity of REEs in terms of their loading properties, which recovered rare earth oxalate from the eluate using oxalic acid precipitation in acidic medium.

2. Results and Discussion

2.1. Characterization of Prepared Composite

2.1.1. FTIR Analysis

FTIR spectra were used not only to verify the structure of the sorbent through the grafting of phosphonic groups into chitosan particles, nor just to obtain information as to the type of binding and the expected mechanisms through changes in the environments surrounding these groups, but also to verify the stability of the sorbent against the acidic solution used in desorption studies (in the sorption–desorption cycles).

Figure 1 shows the FTIR spectra of the magnetite chitosan nanoparticles after being functionalized by amino phosphonate moieties, after loading with metal ions, and after five cycles of sorption–desorption. Figure 1 shows several peaks related to phosphonate groups, which are not found in the non-functionalized particles. Peaks can be seen at 1421 cm^{-1} and 1348 cm^{-1} , 1053 cm^{-1} , and 561 cm^{-1} and 484 cm^{-1} and represent $\text{P}=\text{O}$ (asym.), $\text{P}(\text{O})$ (phosphate(str.)) and $\text{P}-\text{O}-\text{C}$ (str.) sharing with $\text{Fe}-\text{O}$ [81–83] respectively. Most of these peaks are decreased in their intensity by the effect of metal adsorption and have some shifts, while they are restored to their original state after desorption, emphasizing the high stability of the sorbent against degradation processes and its good resistance against acid in the elution procedures. Peaks at 3412 , 3267 , 3274 and 3263 cm^{-1} for MCH, CH-POH, CH-POH+Nd and after five cycles, respectively, are related to OH and NH groups in the chitosan and amino phosphonate groups [84–86].

From Figure 1, we can see, through the shifts and changes towards a lower transmittance, that OH, NH, and P-O, are the groups most noticeably affected by metal ion sorption. This indicates that these groups are used for binding with metal ions. The spectra of the sorbent after desorption are closed to the original functionalized material, which emphasizes the remarkable stability of this composite toward acidic environments and also highlights the reversal sorption. Table S1 shows the most significant peaks in the magnetite chitosan nanoparticles (MCH), phosphonate sorbent (CH-POH), after Nd(III) sorption and after five cycles of sorption–desorption, while Figure S1 shows the full range of the FTIR spectra.

2.1.2. TGA Analysis

Thermal degradation of the functionalized sorbent shows four loss stages against the three stages of the MCH shown in Figure 2. The stabilization plateaus of the loss for both the sorbents were noticed at temperatures of around 450 and $670\text{ }^{\circ}\text{C}$ for MCH and CH-POH, respectively. The final weight losses for both sorbents reached 74.726 and 46.96% respectively. This indicates that the phosphonate groups support the resistance of the thermal degradation (the stabilization was performed at $650\text{ }^{\circ}\text{C}$) and the successive grafting, through an increase in the residual ratio of the hydrocarbons compared with

the original moiety that was supported by amino phosphonic groups (46.96 for magnetite chitosan against 74.726 for functionalized polymer).

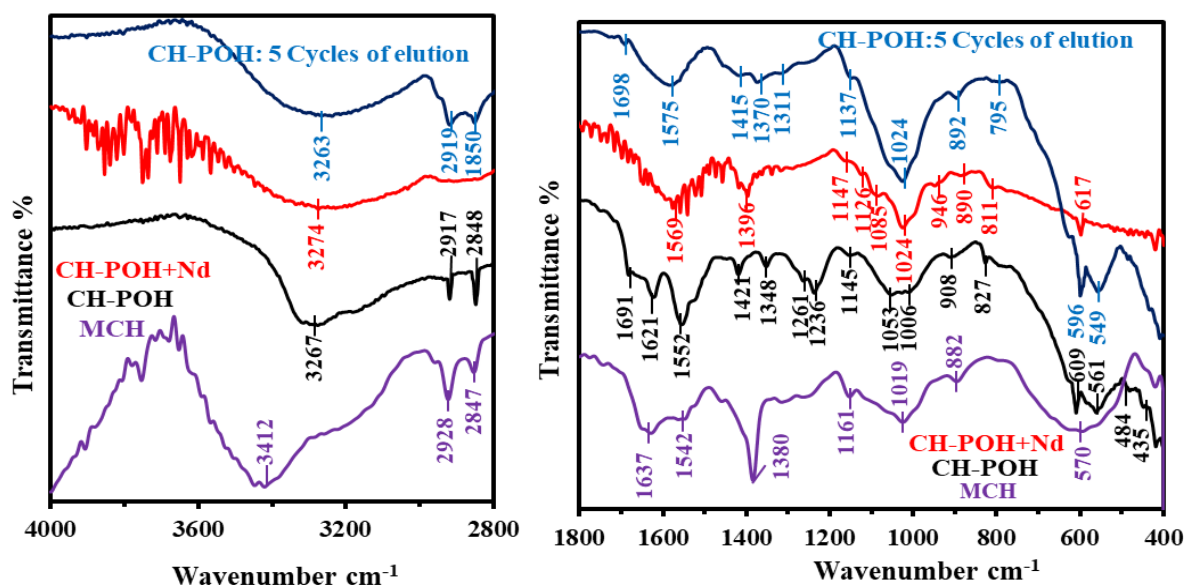


Figure 1. FTIR spectra of MCH, CH-POH, CH-POH+Nd, and after five cycles of sorption–desorption.

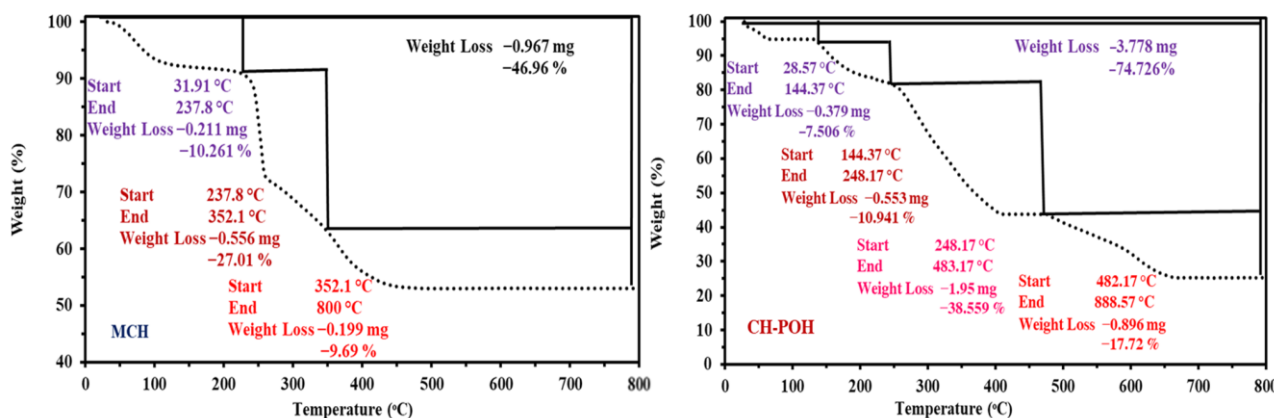


Figure 2. TGA analysis of MCH and CH-PO sorbents.

The loss profiles are discussed in detail as follows. (a) The first loss stage is related to external and internal water release and has a loss percentage of 7.506% at 144.37 $^{\circ}\text{C}$ for CH-POH, while it was recorded at 237.8 $^{\circ}\text{C}$ with a loss percentage of 10.26% for MCH composite. (b) The second loss stage concerns the depolymerization of polysaccharide chains, this was performed at a temperature of 248.17 $^{\circ}\text{C}$ with a loss percentage of 10.94% for CH-POH and 352.1 $^{\circ}\text{C}$ with a loss percentage of 27.01% for MCH. (c) The third stage of degradation concerns the loss of amines and hydroxyl groups and was performed at 483.17 $^{\circ}\text{C}$ with a loss percentage of 38.559% for CH-POH. This stage was the last for MCH with a loss percentage of 9.69%. The last stage of the CH-POH sorbent was related to the degradation of the phosphonate groups (thermal resistance compounds), the organic skeleton (formation of char) and the magnetite particles and showed a loss percentage of 17.72%. Figure S2 shows the DrTG of both sorbents, indicating three bands with different positions at 75.97 $^{\circ}\text{C}$, 254.8 $^{\circ}\text{C}$, and 370.3 $^{\circ}\text{C}$, against 397.3 $^{\circ}\text{C}$, 476.5 $^{\circ}\text{C}$ and 652.5 $^{\circ}\text{C}$ for MCH and CH-POH, respectively.

2.1.3. BET and pH_{PZC} Properties

The functionalized sorbent has an S_{BET} (specific surface area), according to BET measurements (depending on N sorption desorption isotherms), of around 23.85 $\text{m}^2 \text{g}^{-1}$, while

V_p (the porous volume) is around $8.32 \text{ cm}^3 \text{ STP g}^{-1}$. The average pore size is around 126–135 Å.

The acid–base properties of the synthesized sorbents were identified using the surface charge characterization (pH_{PZC}). The sorbents were tested in two different concentrated solutions (0.1 and 1 M NaCl). The data are reported in Figure 3, which shows two identical curves for the same sorbent. The pH_{PZC} was recorded at 6.58 and 6.82 for 0.1 and 1 M NaCl, respectively, for CH-POH, while it was noticed at 6.23 and 6.28 with the same respective concentrations for MCH. The basic properties of these sorbents are related to the pK_a of hydroxyls and amines (for the MCH)—which are increased by grafting and by supporting the phosphonate groups (in case of CH-POH)—and it is this which is primarily responsible for the shifts of the pH to more basic levels (compared with those of chitosan magnetite 6.23 [87]).

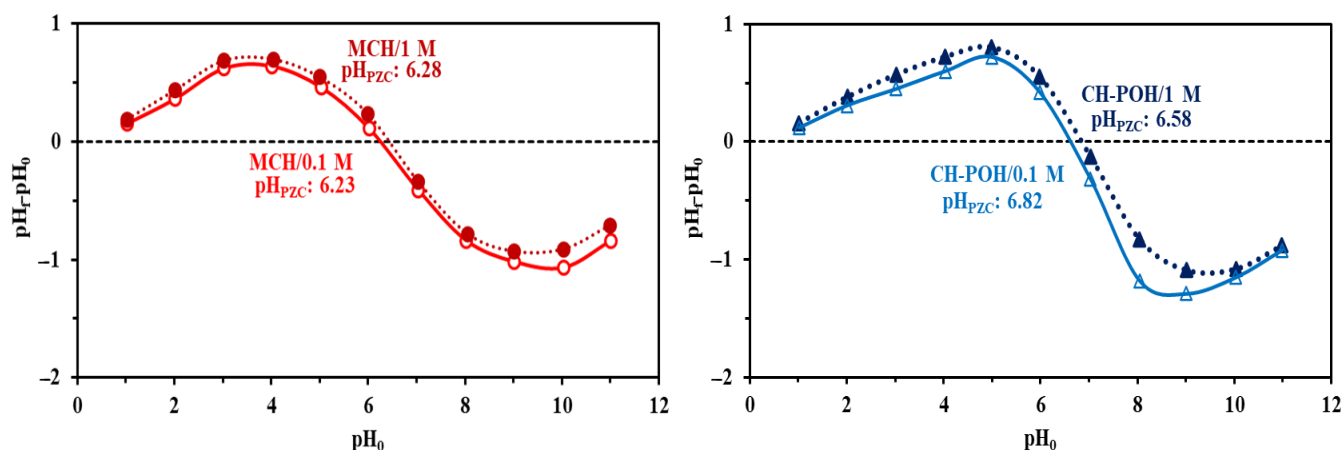


Figure 3. pH_{PZC} of MCH and CH-POH at 0.1 and 1 M NaCl.

2.1.4. Morphology and Textural Properties

Figure 4a,c shows a TEM analysis photograph of the pristine and phosphorylated composites, which appear as magnetite nanoparticles of irregular embedment (appearing as dark points with diameters ranging from 2 to 15 nm for both sorbents). This spreads as a heterogeneous shape inside the polymer composite. The size of the magnetite is around $7 (\pm 2)$ nm. Figure 4b,d show an SEM photograph of the same respective sorbents. The overall size of the particles is less than one micron, which appear as irregular shapes.

2.1.5. Elemental Analysis (EA)

Table S2 shows the EA of chitosan nanoparticles before and after the grafting of phosphorylated groups. There is a noticeable increase in percentage of N and O from 4.12% (2.94 mmol) to 5.58% (3.98 mmol) and 30.22% (18.89 mmol) to 36.92% (23.08 mmol) for MCH and CH-POH, respectively. The main source of this increase was determined to be the amino phosphonate grafted moieties, which contain N:O:P and C with ratios 1:3:1 and 2% respectively. Additionally, the percentage of P for the final sorbent was shown to be 2.95% (0.95 mmol). This emphasizes the successful grafting of phosphonate groups in the chitosan particles.

Figure 5 shows the EDX analysis (semi-quantitative) of both magnetite chitosan before and after the grafting of phosphonate moieties. It can be seen that the results are in line with the elemental analysis results. Increases in N, O and P contents confirm the successful grafting of the amino phosphonate groups to the surface of the chitosan. The N, O, and P increased from 4.11%, 34.55% and 0% for the MCH to 5.42%, 36.48% and 2.11% for MCH-NPOH.

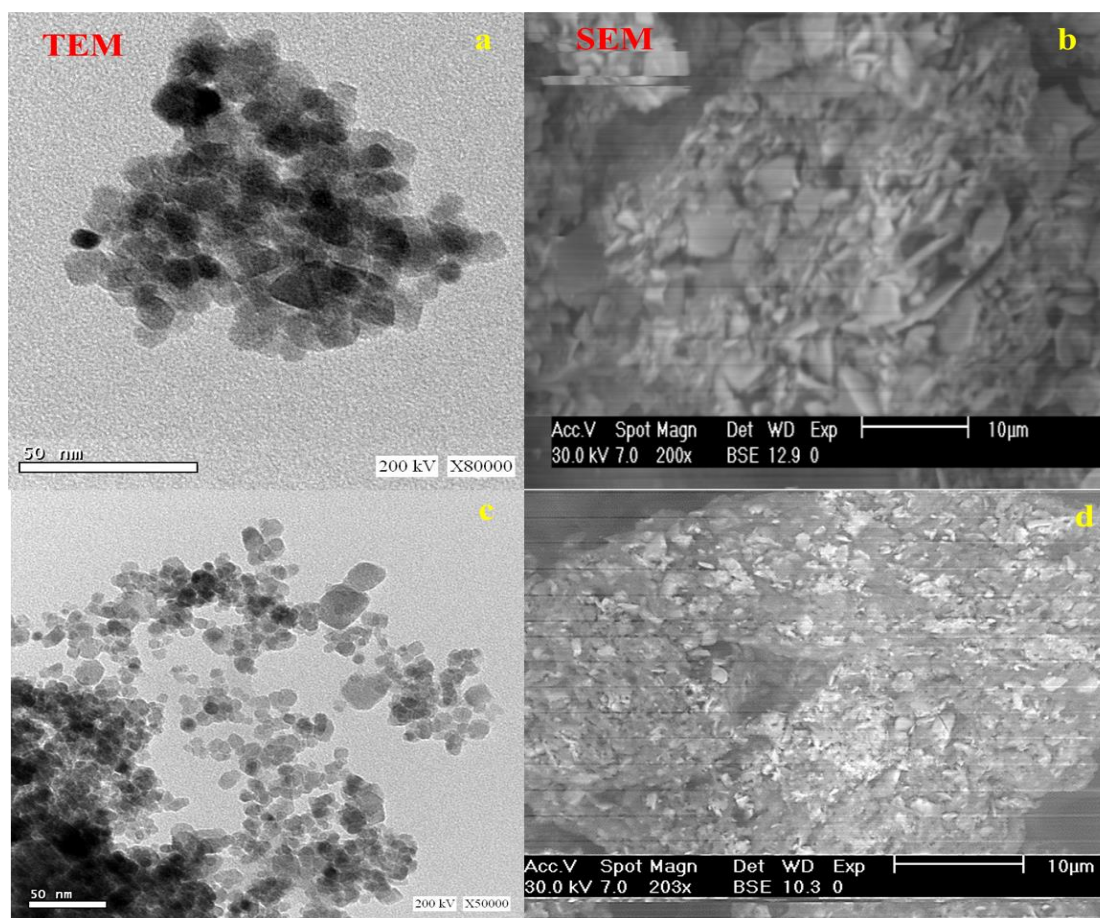


Figure 4. TEM and SEM analyses of MCH (a,b) and CH-POH (c,d) sorbents.

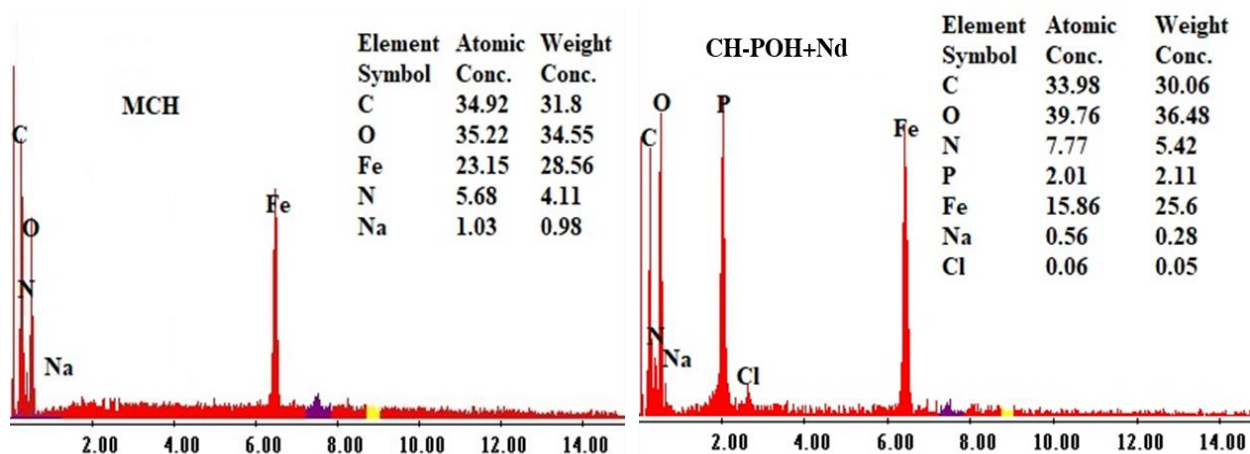


Figure 5. EDX analysis of MCH and CH-POH sorbents.

2.2. Loading from Synthetic Solutions

2.2.1. Effect of pH

Figure 6 shows the Nd sorption properties using CH-POH at different pH_0 (1–6) under visible light and UV emission. The sorption experiments were performed three times and the average, with error bars, are exhibited in the figures. It can be seen that both sorbents have the same sorption profiles (the capacity begins low and increases with pH). It is noteworthy that the sorbent has low sorption capacity in acidic conditions, compared with the slightly acidic medium. This is due to repulsion of the positively charged metal ions (mainly Nd^{3+} or $NdSO_4^+$) and protonated functional groups (mainly; OH, P(OH) and NH_2).

Additionally, with increasing pH the positive charge on the functional groups gradually decreased (partial deprotonation of the sorbent) and the repulsion consequently decreased, allowing for easier binding with the functional groups. The sorption was performed below the pH_{pzc} , in which the sorbent still partially protonated. The sorption stabilized at pH_{eq} 4 for both experiment conditions, wherein the average q_{max} is around $0.79 \text{ mmol Nd g}^{-1}$ and $0.88 \text{ mmol Nd g}^{-1}$ for visible light and UV, respectively. Figure S3 exhibits the speciation diagram of Nd under experimental conditions. The anionic species $(\text{Nd}(\text{SO}_4)_2)^{2-}$ co-existed only at $\text{pH} < 3$, without exceeding 15%, revealing the sorption with the protonated groups. This also demonstrates that the species were mainly present at pH 4 are Nd^{3+} and NdSO_4^+ , while the precipitation was noticed at pH_0 7.25.

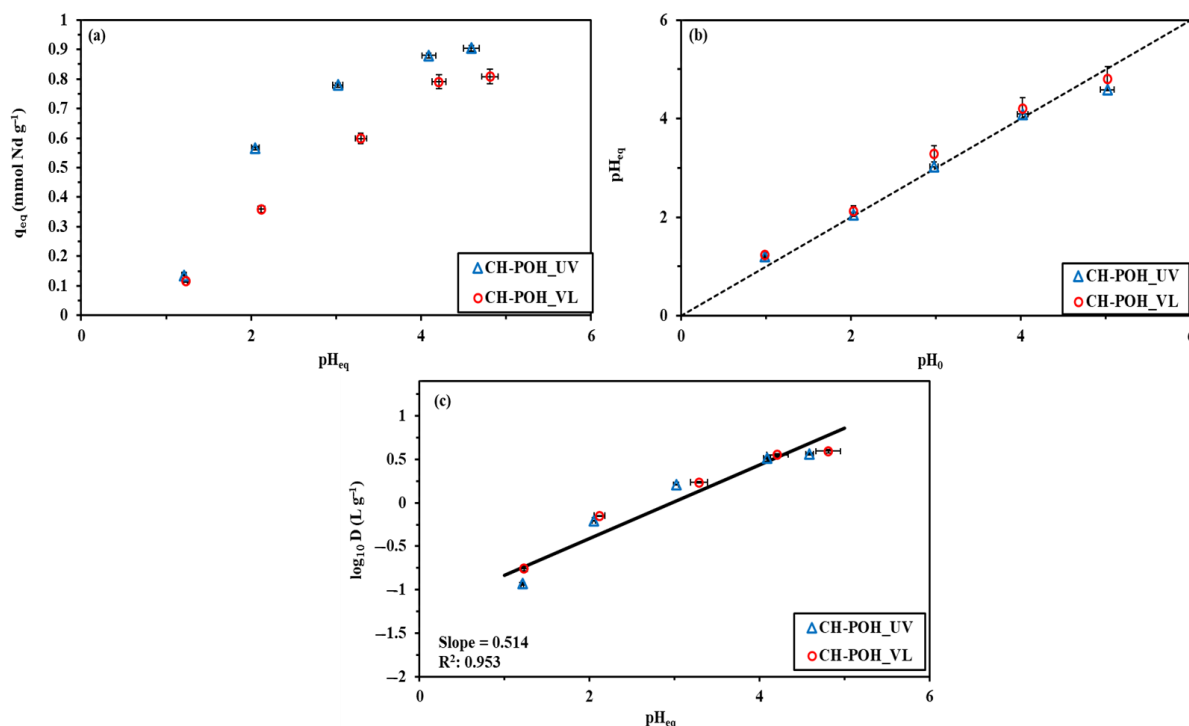


Figure 6. Effect of pH_{eq} on Nd sorption capacity (a), pH diagram (pH_{eq} against pH_0) (b), and the plotting diagram of $\text{Log}_{10}D$ and pH_{eq} (c) using CH-POH sorbent under visible light and UV (C_0 : $0.36 \text{ mmol Nd L}^{-1}$; sorbent dose, SD: 0.66 g L^{-1} ; time: 48 h; v : 210 rpm).

Figure 6b, reports the average and the error bar of the changes to pH during neodymium sorption under both experimental procedures (UV and VL). Both processes exhibit the same profiles, wherein the UV emission produces the highest changes to pH. By comparing these data with those obtained from the pH_{pzc} experiment, it was observed that the variation of the pH in the presence of metal ions is less marked than in their absence. From these data it was concluded that the sorption was performed by releasing protons from the phosphonic groups during the sorption of REEs.

Figure 6c includes the plotting of $\log_{10} D$ (D is the distribution ratio equivalent to $q_{\text{eq}}/C_{\text{eq}}$) vs. pH_{eq} . The slope from this plot is close to 0.51 and 0.57 for both sorbents. This means that the sorption mechanism was performed through an ionic exchange mechanism using two protons from the sorbent per metal ion (probably mainly with sulfate species, as appeared in the EDX analysis in Figure 7 (the presence of S element in the spectra)).

Figure S4 shows the EDX analysis of the loaded sorbent at pH_{eq} 4. This represents a high percentage of Nd (3.46%) and reflects the high affinity of this composite toward REEs. The spectra show the presence of S element (which is absent from the original functionalized sorbent; see Figure 5), which confirms the sorption of Nd in a sulfate species beside a trivalent ion. Additionally, the oxygen percentage was increased from 36.48%

before loading to 37.21% after Nd sorption, the source of O in this case being provided from the sulfate species.

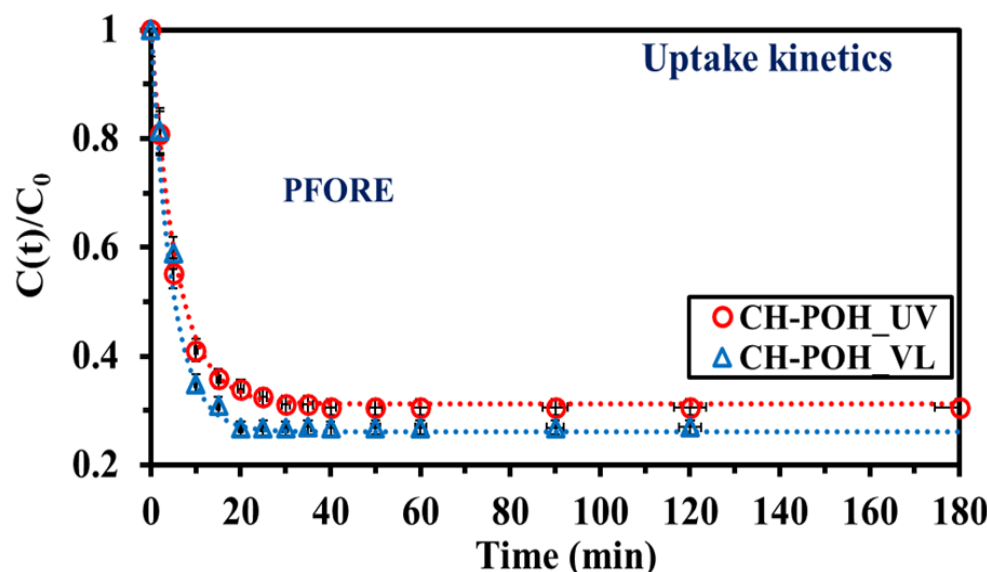


Figure 7. Uptake kinetics fitted by PFORE for Nd(III) using CH-POH under visible light and UV conditions (pH_0 : 4; C_0 : 0.36 mmol Nd L^{-1} ; SD: 0.66 g L^{-1} ; T: 21 ± 1 °C; v: 210 rpm).

2.2.2. Uptake Kinetics

The kinetics profiles may be controlled by different parameters, such as resistances to diffusion (film, intraparticle diffusion and bulk modes). The resistance to bulk diffusion and the effects of the film diffusion are limited by proper agitation speed, which causes a homogenous sorbent and solute distribution. The experimental profiles were fitted using different reaction rates associated with pseudo-first-order rate equations (PFORE) as shown in Figure 7, pseudo-second-order rate equations (PSORE) (Figure S5a), and the resistance to intraparticle diffusion (RIDE), (Figure S5b). The PFORE is considered to be a well fitted equation for the experimental profiles for UV and VL conditions, as shown in Figure 7, while the other equations are poorly fitted for the experimental profiles, as shown in Figure S5.

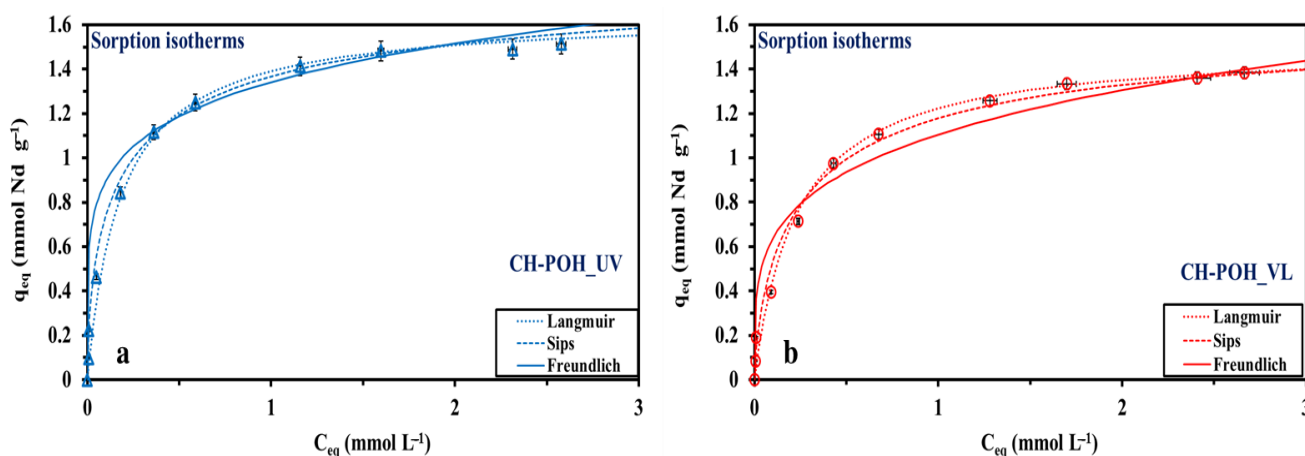
It is noteworthy that the PFORE have closer determinations through a comparison of the equilibrium capacities (i.e., of the sorption capacities in comparison with those obtained from the experimental studies): the $q_{\text{eq},1}$ is overestimated with the $q_{\text{eq},\text{exp}}$ in both experimental conditions. From the kinetic profiles, we see that the sorbent shows a total sorption within 20 min, in which around 85% of the sorption was performed in the first 10 min. From these data we can confirm that the sorption was mainly performed on the surface (external layer) and then, to a small extent, in the pores (which is limited). Table 1 reports the comparison of the models' parameters. By comparing the q_{exp} (the calculated sorption capacities value), AIC and the rate coefficients (R^2), we see a remarkable preference of the PFORE (physical sorption) compared with the chem-sorption of the PSORE.

2.2.3. Sorption Isotherms

The importance of the sorption isotherms is in their ability to detect the maximum sorption capacities (from sorbent saturation) and the sorbent affinity coefficient toward the selected metal ions. The sorption isotherms performed at an initial pH 4 for both sorption conditions (UV and VL). The saturation plateaus began around 1.5 and 1.2 mmol L^{-1} for UV and VL, respectively. The maximum loading capacities were recorded as 1.45 mmol Nd g^{-1} and 1.33 mmol Nd g^{-1} for the respective experiments. On the other hand, a significant increase of initial slopes under UV conditions emphasizes the improvement of the sorption performances. The different profiles applied for sorption isotherms were Langmuir, Freundlich and the Sips equations, as shown in Figure 8.

Table 1. Uptake kinetics of the Nd(III)sorption using CH-POH sorbent under UV and VL parameters.

Model	Parameter	Unit	CH-POH#UV	CH-POH#VL
PFORE	$q_{eq,exp}$	mmol Nd g^{-1}	0.871	0.779
	$q_{eq,1}$	mmol Nd g^{-1}	0.891	0.785
	$k_1 \times 10$	min^{-1}	0.395	0.582
	R^2	-	0.996	0.991
	AIC	-	−102	−95
PSORE	$q_{eq,2}$	mmol Nd g^{-1}	1.08	0.886
	$k_2 \times 10$	$\text{gmmol}^{-1} \text{ min}^{-1}$	1.95	2.36
	R^2	-	0.893	0.902
	AIC	-	−52	−44
RIDE	$D_e \times 10^8$	$\text{m}^2 \text{ min}^{-1}$	2.16	1.86
	R^2	-	0.928	0.953
	AIC	-	−87	−89

**Figure 8.** Sorption isotherms of Nd(III) using CH-POH at (a) UV and (b) VL using Langmuir, Sips and Freundlich equations (pH_0 : 4; C_0 : 0.05–3.3 mmol Nd L^{−1}; SD: 0.66 g L^{−1}; T: 21 ± 1 °C; v: 210 rpm; time: 48 h).

The Freundlich (power-type equation) was used for multi-layer sorption. A heterogeneous distribution was expected between the molecules. This is usually recognized by a non-asymptotic shape. The Langmuir equation (homogeneous sorption) is assumed to occur through a monolayer and is performed without the interactions of the sorbed molecules. Consequently, it is more fitting for the experimental profiles. The Sips equation (a combination of the Langmuir and Freundlich equations) is performed by the addition of an adjustable parameter (n) to make the experimental profiles more fitting. Table 2 represents the parameters of the three models. By comparison of the R^2 and AIC, it was shown that the Langmuir and Sips are the most well fitted equations for the experimental profiles, displaying improved performance over the Freundlich equation. The high affinity of the sorbent toward REEs can be explained by the nature of the reactive group activities and the metal ion softness character. Additionally, according to Pearson's rules, the hard and the soft acid–base theory (HSAB) [88,89] assigns a high affinity and reactivity of hard acids to the hard bases. The phosphonate groups are classified as hard bases [90] and have a high affinity to REEs (classified as hard acids).

Table 3 reports the sorption capacities and the sorption properties of alternative sorbents in the literature for comparison with the CH-POH sorbent. Different conditions sometimes make such comparison difficult; however, it still demonstrates meaningful trends. The CH-POH sorbent shows relatively high sorption capacities in comparison with most in the literature. Some sorbents have been reported to have high sorption capacities, such as calixarene-functionalized graphene oxide composite [91], poly- γ glutamic acid

sorbent [92], and carboxylic acid modified corn stalk gel [93], but CH-POH is preferential in terms of kinetic characteristics and affinity coefficients.

Table 2. Sorption isotherms of Nd(III) using CH-POH sorbent under UV and VL.

Model	Parameter	Unit	CH-POH_UV	CH-POH_VL
Langmuir	$q_{m,exp}$	$mmol\ Nd\ g^{-1}$	1.45	1.33
	$q_{m,L}$	$mmol\ Nd\ g^{-1}$	1.49	1.36
	b_L	$L\ mmol^{-1}$	3.68	2.25
	R^2	-	0.991	0.989
	AIC	-	-130	-124
Freundlich	k_F	$L^{1/n_F}\ mmol^{1-1/n_F}\ g^{-1}$	1.37	1.95
	n_F	-	2.86	2.53
	R^2	-	0.855	0.872
	AIC	-	-39	-43
Sips	$q_{m,S}$	$mmol\ Nd\ g^{-1}$	1.51	1.42
	b_S	$(L\ mmol^{-1})^{1/n_S}$	1.66	1.59
	n_S	-	0.962	0.901
	R^2	-	0.995	0.990
	AIC	-	-153	-133

2.2.4. Binding Mechanism

The data collected from the pHpzc (for the surface charge of the sorbent), FTIR (the used functional groups in the binding mechanisms, through changes in their intensities and displacement), speciation diagram of neodymium ions and the studies of the pH effect, provided a prediction of the sorption mechanism. From the experimental conditions, it was found that the maximum adsorption of Nd(III) ions is achieved in slightly acidic pH (around 4) with partial deprotonation of functional groups (from the pHpzc). This collection of functional groups (OH, NH, P-OH and P=O) exhibit an electrostatic attraction with positively charged metal ions and the availability of a lone pair of electrons on these groups makes chelation properties possible. The sharing of these functions was emphasized through the FTIR (change in intensities) of NH and OH bands and the displacement of some functional groups, such as P=O, indicating a change in the environment surrounding these groups that is used for binding. The slope of the plot of $\log_{10} D$ vs. pH_{eq} gives data close to 0.51 and 0.57 for both sorbents. This indicates that the ionic exchange mechanism was performed with the expectation of two protons from the sorbent per one of the metal ions as shown in Scheme 1.

2.2.5. Selectivity from Multi-Component Aqueous Solutions

The sorbent was transferred to test the selectivity (as a first stage, prior to application) toward metal ions in a multi component equimolar system for the possible extraction of REE from polymetallic solution. These complementary studies were performed with most of the elements associated with REEs in the leachate solutions (i.e., Ca, Mg, Fe, and Al). These elements are found mostly in sedimentary rocks such as shale and gibbsite ore materials. The sorption performances were evaluated at different pH values (ranging from 1 to 5). From Table 4, it can be seen that the sorbent has a high affinity toward REEs at slightly alkaline pH as opposed to representative and transition metals. The data from selectivity coefficients $SC_{Me1/Me2} = D_{Me1}/D_{Me2}$, shows a preference for Nd over other metals.

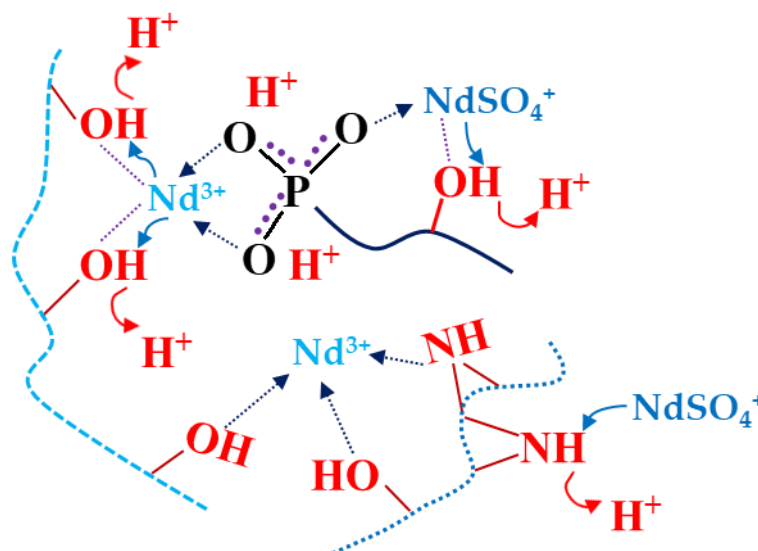
At pH_{eq} 4.86, the selectivity of the CH-POH has the following sequence.

Al(III) (SC: ~34.8) \approx Ca(II) (SC: ~34.4) \gg Mg(II) (SC: ~22.2) \gg Fe(III) (SC: ~13.4) in visible light, this selectivity was changed and improved by using UV emission, which obtained a sequence of Mg(II) (SC: ~58) $>$ Ca(II) (SC: ~53.8) $>$ Al(III) (SC: ~50.1) \gg Fe(III) (SC: ~19.6).

Figure S6 shows the total capacity of the sorbent toward these metal ions at different pH conditions. This figure emphasizes the improved capacity and selectivity effected by the pH and UV conditions.

Table 3. Nd(III) sorption properties with a comparison of performances (equilibrium time, pH, $q_{m,L}$ and b_L).

Sorbent	pH	Equilibrium Time (min)	$q_{m,L}$ (mmol g ⁻¹)	b_L (Lmmol ⁻¹)	Reference
Ion-imprinted composites	7.7	10	0.24	175	[94]
<i>Sargassum</i> -sp.	5	180	0.70	27.77	[95]
<i>Kluyveromyces marxianus</i> .	1.5	1440	0.083	5.63	[96]
Phosphorus sol-gel	6	180	1.13	-	[97]
Impregnated magnetic microcapsules	4	600–720	1.04	4904	[98]
Calixarene-functionalized with graphene oxide	7	240	2.16	3.38	[91]
Cysteine-magnetite-NPs	7	30	0.59	261.4	[99]
Silica impregnated with IL	3.5	200	0.145	267	[100]
Fumarated- polystyrene	5	50	0.30	5.87	[101]
<i>Chlorella-vulgaris</i>	5	30	0.87	4.18	[102]
Poly γ -glutamic acid	3	-	1.64	8.47	[92]
Graphitic C ₃ N ₄ -nanosheets	8	360	0.91	140	[103]
Carboxylic functionalized corn stalk gel	3	360	2.44	591	[93]
Diatomaceous-earth	5	150	1.17	26.1	[104]
Lanthanide-MOF	6	120	0.99	5.19	[105]
Mesoporous functionalized sorbent	5	40	1.06	1.24	[106]
Phosphorylated chitosan composite under UV	4	20	1.49	3.68	<i>This work</i>
Phosphorylated chitosan composite under VL	4	20	1.36	2.25	<i>This work</i>



Scheme 1. Expected binding mechanisms for Nd(III) sorption on CH-POH sorbent.

Table 4. Selectivity studies of CH-POH in polymetallic equimolar solution under VL(a) and (UV) conditions.

pH _{eq}	VL				UV			
	Nd/Fe	Nd/Ca	Nd/Mg	Nd/Al	Nd/Fe	Nd/Ca	Nd/Mg	Nd/Al
1.1	0.154	1.173	0.428	0.574	0.201	0.630	0.8278	0.531
2.12	4.118	5.578	3.781	6.344	3.665	7.193	4.934	9.321
3.18	6.2098	15.971	9.602	14.599	4.867	17.647	12.475	18.958
3.76	15.3938	34.587	22.628	32.78	16.388	44.328	51.68	44.212
4.75	13.385	34.481	22.213	34.789	19.561	53.803	58.013	50.147

2.2.6. Metal Desorption and Sorbent Recycling

The desorption process of adsorbed Nd(III) was achieved using an acidic condition of 0.2 M HCl solution as eluent. The desorption procedures seem faster than the sorption process (the loading processes were performed during 20 min of contacts compared with less than 15 min for complete elution of adsorbed metal ions). Around 10 min is considered to be sufficient for elution of more than 80% and 75% of adsorbed metal ions at UV and VL, respectively. From Figure 9, it can be seen that the elution procedures were improved by using UV emission. The data in the figure are the average of the three elution experiments with error bar, in which the loaded samples were collected from the uptake kinetic experiments.

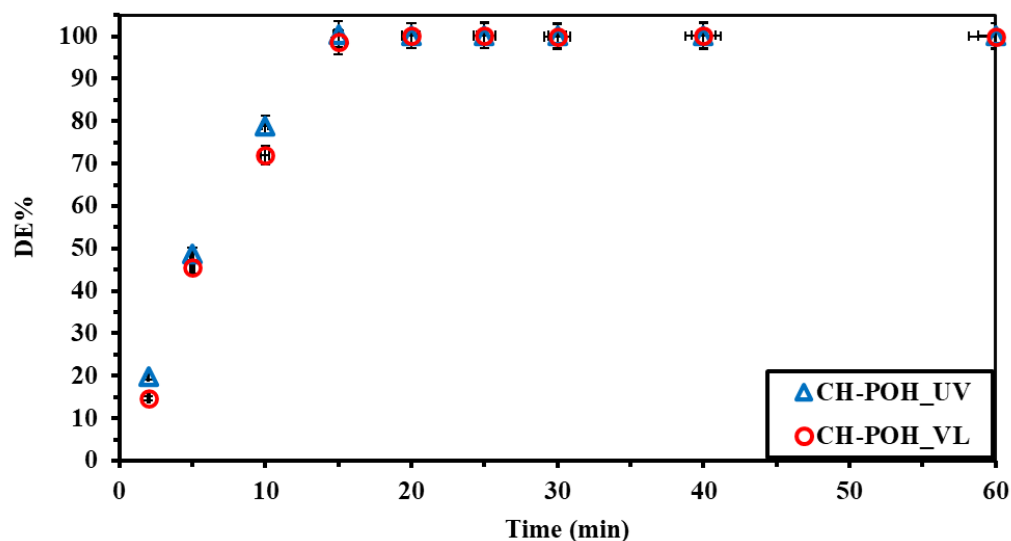


Figure 9. Elution experiments of loaded metal ions using 0.2 M HCl solution.

Table 5 shows the sorption–desorption cycles for five successive runs for possible reuse of the sorbent and for its reproducing properties. The sorption shows a limited decrease in the efficiency for both experiments (less than 3% decrease in the efficiency under UV and VL), while the elution remains around 100% after the five cycles. This reflects the stability of the sorbent toward the sorption–desorption process. This also was emphasized by the FTIR as shown in Figure 1.

Table 5. Recycling data of CH-POH sorbent (SE: the sorption efficiency (%); DE: the desorption efficiency (%); StD: the standard deviation (%)).

Cycle #	SE	StD	DE	StD
1	85.23	0.86	100.0	0.21
2	84.67	1.05	100.0	0.14
3	84.01	0.51	99.78	0.12
4	83.66	0.33	100	0.22
5	83.14	0.21	99.83	0.34

2.3. Application on Ore Leachate

Table 6 shows the concentration of metal ions after leaching from ore materials and applying uranium extraction processes using quaternary ammonium resin. The high concentration of REE (361 mg L^{-1}) in the raffinate supports the authors' proposal to apply it toward extraction and attempt to upgrade the concentration in order to make it suitable for selective precipitation.

The loading experiments were performed under agitation procedures in the presence of UV and VL, and the results are reported in Table 7.

Table 6. Chemical composition of raffinate with extraction % after treatment for U removal.

Constituents	Conc. (mg/L)	Extraction %	Constituents	Conc. (mg/L)	Extraction %
Fe	1814	30.52	Mg	308	12
Al	1989	21.04	REE	361	17.71
Ca	397	11.4			

Table 7. Effect of the pH values on sorption efficiencies of polymetallic ions using CH-POH after treatment with amino-sulfonic chitosan composite.

Conditions	pH _{eq}	Nd/Zr	Nd/Pb	Nd/Mg	Nd/Fe	Nd/Al	Nd/Ca
VL	1.16	12.345	5.4483	5.138	9.138	3.375	6.810
	2.19	7.306	7.1364	3.623	7.883	4.513	8.864
	3.27	11.565	12.461	10.383	19.911	9.197	15.956
	4.11	13.691	23.836	20.360	2.056	8.957	21.552
	4.89	12.567	23.874	23.558	1.424	3.559	24.567
UV	1.11	7.807	6.93	3.697	7.04	3.988	6.912
	2.15	10.029	14.255	3.613	11.313	7.861	9.65
	3.21	12.853	11.369	7.61	20.588	12.378	10.273
	4.1	14.243	26.82	17.862	2.305	12.42	13.745
	4.79	14.427	30.282	27.54	1.98	3.918	18.531

2.4. Extraction Results

The leachate solution from acidic attack of the pristine ore materials produced a poly-metallic solution with high concentration of metal ions, including RREs. Pretreatment of the leaching solution for removal of particular metal ions was performed using quaternary ammonium resin and the produced raffinate solution had a high concentration of REEs that could be valorized. The residual concentration and removal percentage of the most important metal ions are reported in Table 6. The sorbent shows different extraction percentage toward metal ions with different extraction tendencies, in which the loss percentage of REEs is around 17.8% from the original leaching solution.

Different conditions were applied to test the recovery of REEs in the residual solution using the CH-POH sorbent (different values of pH (ranging from 1 to 5) under UV and VL conditions). Table 7 shows the selectivity of the sorption after treatment for the most important metal ions, indicating (a) that the selectivity and sorption capacity are gradually increased with the pH, (b) the high removal of REE compared with major and heavy elements (this is parallel to the results obtained from the selectivity test) and (c) that the selectivity was improved when under UV conditions. The composite remains a useful tool for REEs recovery. The selectivity was recorded under VL with the order $\text{Ca} > \text{Pb} \approx \text{Mg} \gg \text{Zr} > \text{Al} \approx \text{Fe}$ and under UV with the order $\text{pb} > \text{Mg} > \text{Ca} > \text{Zr} \gg \text{Al} \approx \text{Fe}$.

3. Materials and Methods

3.1. Materials

Chitosan (Medium M. Wt, with acetylation degree 75–85%), aminomethyl phosphonic acid (99%), anhydrous sodium hydroxide pellets (98%), ferrous sulfate (99%), ammonium ferric sulfate (>99.9%) and formaldehyde (37%, w%) were supplied by Sigma-Aldrich (Taufkirchen, Germany). Epichlorohydrin (EPI; 99%) was supplied by Shanghai-Makclin, Biochemical Co., Ltd. (Shanghai, China). Neodymium (III) sulfate was purchased by the National Engineering Research Centre (NERC) of Rare Earth Metallurgy and Functional Materials—China. The anhydrous calcium chloride (97%), hydrated salts of aluminum chloride ($\text{AlCl}_3 \cdot 6\text{H}_2\text{O}$; 98%), magnesium chloride ($\text{MgCl}_2 \cdot 6\text{H}_2\text{O}$; 95%), and ferric chloride ($\text{FeCl}_3 \cdot 6\text{H}_2\text{O}$; 97%) used in the selectivity tests were purchased through the Guangdong Guanghua-Sci, Tech Co., (Shantou, China). Acetone (99%), ethanol (95%) and absolute ethanol were supplied from Xilong-Scientific Co., Ltd., (Shantou, China). Other reagents were produced from Prolabo-products (VWR-Radnor; PA, USA).

3.2. Characterizations

The FT-IR spectra (range 4000–400 cm^{-1}) were achieved for the dried sorbents (60 °C) after grinding with KBr; 1% (*w/w*), and designed as KBr disk using Shimadzu, IR-Tracer, 100-FTIR spectrometer (Shimadzu-Tokyo, Japan). The C, N, P and H contents were analyzed through elemental analysis using 2400 Series II CHNS/O elemental analyzer; PerkinElmer–Waltham (MA, USA). The thermal decomposition of the sorbent was performed under a nitrogen environment with a temperature ramp (10 °C min^{-1}) using TG-DTA; Netzsch-STA449-F3 Jupiter; NETZSCH, Gerätebau, HGmbH, (Selb, Germany). The surface morphology was analyzed via scanning electron microscope; SEM with model Phenom-ProX; Thermo-Fisher Scientific (Eindhoven, The Netherlands), the semi-quantitative analyses were achieved by energy dispersive X-ray; Phenom-ProX, SEM. The concentration of metal ions was detected using ICP-AES; ICPS,7510; Shimadzu (Tokyo, Japan). The pH_{PZC} analysis was measured using pH-drift [107], about 0.1 g of dried sorbent was agitated in 50 mL solution (0.1 M NaCl) for 24 h and the equilibrium pH (pH_{eq}) was measured, the pH of the solution ranged from 1 to 14. The pH_{PZC} was known as $\text{pH}_0 = \text{pH}_{\text{eq}}$. The BET surface area was measured through nitrogen sorption–desorption using Micromeritics Tristar II; Norcross (Gwinnett, GA, USA), with the samples firstly degassed at 120 °C/12 h. The pH of the solution was calibrated by pH iono-meter, S220 Seven; Mettler-Toledo (Shanghai, China). The concentration of metal ions in the solution was measured using the ICP tools (inductively coupled plasma atomic emission spectrometer) by ICPS; 7510; Shimadzu (Tokyo, Japan). The particle size of the synthesized sorbent was investigated by TEM analysis using JEOL-1010, JEOL-Ltd. (Tokyo-Japan).

3.3. Synthesis of Functionalized Sorbent

3.3.1. Synthesis of Magnetite Nanoparticles

Preparation of magnetite nanoparticles was undertaken by thermal precipitation technique through reaction of ferrous sulfate (5 g) and ammonium ferric sulfate (17.35 g) in 50 mL aqueous solution. The mixture undergoes vigorous stirring till dissolved completely. The precipitation was obtained by pH adjustment to 11 using 7 M NaOH solution and the temperature was maintained at around 50 °C for 1 h. The precipitated magnetic nanoparticles were collected from the solution, washed several times by water and acetone then dried at 60 °C overnight.

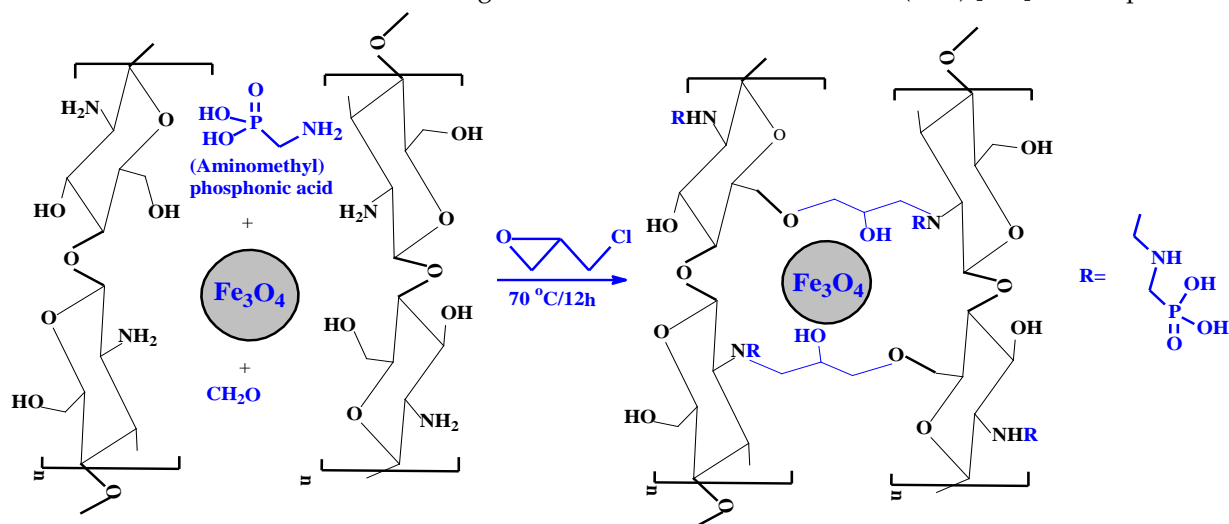
3.3.2. Functionalization of the Nanoparticles

Chitosan particles were dissolved (1 g) in 50 mL of 7% *w/w* acetic acid solution. One gram of (aminomethyl)phosphonic acid (99%) was added to the solution with continuous stirring at 45 °C till complete dissolution, followed by addition of 1 g of formaldehyde dropwise and 2 g of the prepared magnetite nanoparticles. The flask was equipped with a condenser and refluxed to 90 °C for 5 h, after cooling, a further 2 mL epichlorohydrin was added to the mixture and refluxed for a further 7 h. The content of the flask was poured into an aqueous solution of 2% NaOH and was left stirring overnight. The precipitated product was filtered, washed with acetone and water then air dried at 65 °C for 10 h to yield amino phosphonic chitosan nano particles (Scheme 2).

3.4. Metal Sorption from Synthetic Solutions

The sorption experiments were achieved through batch techniques, in which an amount of synthesized composite (m, g) was mixed with a volume of solution (V, L) which containing an initial metal concentration (C_0 , mmol L^{-1}) at an initial pH (pH_0), both of which are variable depending on the experimental conditions and maximum loading (see below). The agitation velocity was fixed at 165 rpm with a temperature 21 ± 1 °C for most experiments. After sorption, the samples were collected and filtered before ICP analysis to detect the final concentration (C_{eq} , mmol L^{-1}). The loading capacity (q_{eq} , mmol g^{-1}) was measured using the mass balance equation $q_{\text{eq}} = (C_0 - C_{\text{eq}}) \times V/m$. The desorption experiment was performed using the batch method with a solution of 0.2 M HCl. The

desorption kinetics (as a function of time) were measured on the samples collected from kinetic experiments and treated with eluent. The sorbent recycling was investigated for five cycles, with a rinsing with water performed between each sorption and desorption step. The sorption isotherms and kinetics were studied by conventional equations that are summarized in Table S3a (Freundlich, Sips and Langmuir equations) and Table S3b (pseudo-first-order rate equation (PFORE), pseudo-second-order rate equation (PSORE), and resistance to intraparticle diffusion (RIDE)). The fitting quality of the curves was determined through the Akaike information criterion (AIC) [108] and R^2 parameters.



Scheme 2. Synthesis of amino phosphonic chitosan nanoparticles.

3.5. Treatment of Ore Material

The samples enriched with rare earth elements were collected after ore processing and extraction of particular elements. The reprocessed leaching liquor still had a high concentration of rare earth element (over 350 mg L^{-1}). The chemical composition of ore materials is identified in Table S4. The produced raffinate after extraction still had a high concentration of rare earth elements that could be valorized. The leaching solution was produced by the effect of acidic attack with the condition of the mixture being 15% H_2SO_4 and 0.25 M NaCl. The suitable ratio of solid/liquid was assigned to 1/2 with an agitation time of 2 h at 90°C . The concentration of the most important elements is shown in Table S5, while Table 6 shows the leaching composition after treatment of the leaching liquor by quaternary ammonium resin for the extraction process.

4. Conclusions

A new functionalized chitosan sorbent bearing phosphonic groups was used to support the sorption process of REEs in mild acidic conditions. The sorbent was designed as a nano structure using magnetite nano particles. The structure of the sorbent was investigated using FTIR, SEM-EDX, TGA, BET, pH_{pzc} , and EA. The sorption procedures were investigated toward Nd(III) ions under visible light and UV emission. The functionalized sorbent shows a high sorption capacity with 20 min required for complete saturation. Kinetic profile was fitted with the PFORE fitted equation. The sorption experiments were performed at slightly acidic conditions (pH 4) with partially protonated properties of the sorbent surface. Using the UV tools caused an improvement of the sorption properties and kinetic efficiency. The sorbent shows highly sorption properties when compared with those found in the literature and appears to be stable against acidic eluents, making it a novel tool for the recovery of REEs from solution. Desorption was achieved by 0.2 M HCl solution, which seems to be fast and sufficient to remove all adsorbed metal ions from the surface, and complete desorption was achieved within 15 minutes. Langmuir and Sips are the most fitted profiles for the sorption isotherms. The sorbent shows stability in

terms of sorption–desorption cycles after five runs of loading and elution procedures. The sorbent shows selectivity in a poly-metallic equimolar solution and UV conditions are more efficient than visible light. The sorbent was used for the recovery of REEs from a raffinate solution after treatment with quaternary ammonium resin. This sorbent appears to be a remarkable tool for REEs recovery.

Supplementary Materials: The following supporting information can be downloaded at: <https://www.mdpi.com/article/10.3390/catal13040672/s1>. Table S1: Assignment peaks of MCH, CH-POH, CH-POH+Nd before and after five cycles of sorption–desorption; Table S2: Elemental analysis of MCH and CH-POH sorbents; Table S3a: Reminder of the equations used for modeling sorption isotherms [18–20]; Table S3b: Reminder of the equations used for modeling uptake kinetics; Table S4: XRF analysis of the study G. El Sela raw materials; Table S5: Chemical composition of the prepared carbonate leach liquor at (pH = 0.3); Figure S1: The full range of the FTIR spectra; Figure S2: DrTG of chitosan magnetite (MCH) and functionalized sorbent (CH-POH); Figure S3: Speciation diagrams for Nd(III) under the experimental conditions; Figure S4: EDX analysis of the CH-POH after Nd(III) sorption; Figure S5: The unfitted profiles of the PSORE and RIDE for CH-POH sorbent, (pH0: 4; C0: 0.36 mmol Cd L⁻¹; SD: 0.66 g L⁻¹; T: 21 ± 1 °C; v: 210 rpm); Figure S6: Total sorption capacity of CH-POH in polymetallic equimolar solution under VL(a) and (UV) conditions [81,109–137].

Author Contributions: Conceptualization, M.F.H., J.W., Y.W. and X.Y.; methodology, M.F.H., J.W. and Y.W.; software, H.M., A.F. and M.S.K.; validation, M.F.H. and H.M.; formal analysis, A.F., M.S.K. and S.N.; investigation, J.W., S.N. and X.Y.; resources, M.F.H. and A.F.; data curation, K.A. and X.Y.; writing—original draft preparation, M.F.H.; writing—review and editing, M.F.H. and A.F.; visualization, A.F., K.A. and H.M.; supervision, M.F.H. and Y.W.; project administration, S.N.; funding acquisition, Y.W. and S.N. All authors have read and agreed to the published version of the manuscript.

Funding: The National Natural Science Foundation of China for supporting projects (U1967218, and 11975082). National Key R&D Program of China (2022YFB3506100).

Data Availability Statement: Data can be obtained from the authors on demand.

Acknowledgments: Y.W. acknowledges the National Natural Science Foundation of China for supporting projects (U1967218, and 11975082). National Key R&D Program of China (2022YFB3506100).

Conflicts of Interest: The authors declare no conflict of interest.

References

1. Tse, P.-K. *China's Rare-Earth Industry*; US Department of the Interior: Washington, DC, USA; US Geological Survey: Asheville, NC, USA, 2011.
2. Hatch, G.P. Dynamics in the global market for rare earths. *Elements* **2012**, *8*, 341–346. [\[CrossRef\]](#)
3. Long, K.R. The future of rare earth elements—will these high-tech industry elements continue in short supply. *US Geol. Surv. Open-File Rep.* **2011**, *1189*, 41.
4. Van Gosen, B.S.; Verplanck, P.L.; Seal, R.R., II; Long, K.R.; Gambogi, J. *Rare-Earth Elements*; 1411339916; US Geological Survey: Asheville, NC, USA, 2017.
5. Zhou, B.; Li, Z.; Chen, C. Global potential of rare earth resources and rare earth demand from clean technologies. *Minerals* **2017**, *7*, 203. [\[CrossRef\]](#)
6. Blinova, I.; Lukjanova, A.; Reinik, J.; Kahru, A. Concentration of lanthanides in the Estonian environment: A screening study. *J. Hazard. Mater. Adv.* **2021**, *4*, 100034. [\[CrossRef\]](#)
7. Paulick, H.; Machacek, E. The global rare earth element exploration boom: An analysis of resources outside of China and discussion of development perspectives. *Resour. Policy* **2017**, *52*, 134–153. [\[CrossRef\]](#)
8. Kannan, U.; Ganesan, S. Dysprosium as a resonance absorber and its effect on the coolant void reactivity in Advanced Heavy Water Reactor (AHWR). *Ann. Nucl. Energy* **2010**, *37*, 270–276. [\[CrossRef\]](#)
9. Charalampides, G.; Vatalis, K.I.; Apostoplos, B.; Ploutarch-Nikolas, B. Rare earth elements: Industrial applications and economic dependency of Europe. *Procedia Econ. Financ.* **2015**, *24*, 126–135. [\[CrossRef\]](#)
10. Mueller, S.R.; Waeger, P.A.; Widmer, R.; Williams, I.D. A geological reconnaissance of electrical and electronic waste as a source for rare earth metals. *Waste Manag.* **2015**, *45*, 226–234. [\[CrossRef\]](#)
11. Hua, Z.S.; Wang, L.; Wang, J.; Xiao, Y.P.; Yang, Y.X.; Zhao, Z.; Liu, M.J. Extraction of rare earth elements from NdFeB scrap by AlF₃-NaF melts. *Mater. Sci. Technol.* **2015**, *31*, 1007–1010. [\[CrossRef\]](#)

12. Tsamis, A.; Coyne, M. *Recovery of Rare Earths from Electronic Wastes: An Opportunity for High-Tech SMEs*; EPRS: Brussels, Belgium, 2015; p. 44.
13. Tan, Q.; Li, J.; Zeng, X. Rare earth elements recovery from waste fluorescent lamps: A review. *Crit. Rev. Environ. Sci. Technol.* **2015**, *45*, 749–776. [\[CrossRef\]](#)
14. Tunsu, C.; Petranikova, M.; Gergoric, M.; Ekberg, C.; Retegan, T. Reclaiming rare earth elements from end-of-life products: A review of the perspectives for urban mining using hydrometallurgical unit operations. *Hydrometallurgy* **2015**, *156*, 239–258. [\[CrossRef\]](#)
15. Tunsu, C.; Petranikova, M.; Ekberg, C.; Retegan, T. A hydrometallurgical process for the recovery of rare earth elements from fluorescent lamp waste fractions. *Sep. Purif. Technol.* **2016**, *161*, 172–186. [\[CrossRef\]](#)
16. Liu, Z.; Li, H. Metallurgical process for valuable elements recovery from red mud-A review. *Hydrometallurgy* **2015**, *155*, 29–43. [\[CrossRef\]](#)
17. Rivera, R.M.; Ulenaers, B.; Ounoughene, G.; Binnemans, K.; Van Gerven, T. Extraction of rare earths from bauxite residue (red mud) by dry digestion followed by water leaching. *Miner. Eng.* **2018**, *119*, 82–92. [\[CrossRef\]](#)
18. Ai-Thyabat, S.; Zhang, P. Extraction of rare earth elements from upgraded phosphate flotation tailings. *Miner. Metall. Process* **2016**, *33*, 23–30.
19. Hammas-Nasri, I.; Horchani-Naifer, K.; Férid, M.; Barca, D. Rare earths concentration from phosphogypsum waste by two-step leaching method. *Int. J. Miner. Process.* **2016**, *149*, 78–83. [\[CrossRef\]](#)
20. Jin, H.-X.; Mao, X.-H.; Li, J.-Q.; Wang, M.-L.; Yang, S. Study on the enrichment and leaching law of rare earth in the circulating acid leaching process of Zhijin phosphate rock. In *Energy and Mechanical Engineering: Proceedings of 2015 International Conference on Energy and Mechanical Engineering; Energy and Mechanical Engineering, Wuhan, China, 17–18 October 2015*; World Scientific: Singapore, 2016; pp. 358–370. [\[CrossRef\]](#)
21. Laurino, J.; Mustacato, J. *The Extraction and Recovery of Rare Earth Elements from Phosphate Using PX-107 and CHELOK® Polymers*; Periodic Products, Inc.: Bartow, FL, USA, 2015; p. 31.
22. Mashkovtsev, M.; Botalov, M.; Smyshlyaev, D.; Pajarre, R.; Kangas, P.; Rychkov, V.; Koukkari, P. Pilot-scale recovery of rare earths and scandium from phosphogypsum and uranium leachates. *E3S Web Conf.* **2016**, *8*, 01026. [\[CrossRef\]](#)
23. Ruiz Canovas, C.; Macias, F.; Perez Lopez, R.; Miguel Nieto, J. Mobility of rare earth elements, yttrium and scandium from a phosphogypsum stack: Environmental and economic implications. *Sci. Total Environ.* **2018**, *618*, 847–857. [\[CrossRef\]](#)
24. Salem, M.; Souissi, R.; Souissi, F.; Abbes, N.; Moutte, J. Phosphoric acid purification sludge: Potential in heavy metals and rare earth elements. *Waste Manag.* **2019**, *83*, 46–56. [\[CrossRef\]](#) [\[PubMed\]](#)
25. Abaka-Wood, G.B.; Zanin, M.; Addai-Mensah, J.; Skinner, W. Recovery of rare earth elements minerals from iron oxide–silicate rich tailings—Part 2: Froth flotation separation. *Miner. Eng.* **2019**, *142*, 105888. [\[CrossRef\]](#)
26. Liu, P.; Huang, R.; Tang, Y. Comprehensive understandings of rare earth element (REE) speciation in coal fly ashes and implication for REE extractability. *Environ. Sci. Technol.* **2019**, *53*, 5369–5377. [\[CrossRef\]](#) [\[PubMed\]](#)
27. Seredin, V.V.; Dai, S.; Sun, Y.; Chekryzhov, I.Y. Coal deposits as promising sources of rare metals for alternative power and energy-efficient technologies. *Appl. Geochem.* **2013**, *31*, 1–11. [\[CrossRef\]](#)
28. Abaka-Wood, G.; Addai-Mensah, J.; Skinner, W. The concentration of rare earth elements from coal fly ash. *J. South. Afr. Inst. Min. Metall.* **2022**, *122*, 21–28. [\[CrossRef\]](#)
29. Lu, X.; Huang, Z.; Liang, Z.; Li, Z.; Yang, J.; Wang, Y.; Wang, F. Co-precipitation of Cu and Zn in precipitation of struvite. *Sci. Total Environ.* **2021**, *764*, 144269. [\[CrossRef\]](#) [\[PubMed\]](#)
30. Vander Hoogerstraete, T.; Binnemans, K. Highly efficient separation of rare earths from nickel and cobalt by solvent extraction with the ionic liquid trihexyl (tetradecyl) phosphonium nitrate: A process relevant to the recycling of rare earths from permanent magnets and nickel metal hydride batteries. *Green Chem.* **2014**, *16*, 1594–1606.
31. Möller, V.; Williams-Jones, A.E. A hyperspectral study (V-NIR-SWIR) of the Nechalacho REE-Nb-Zr deposit, Canada. *J. Geochem. Explor.* **2018**, *188*, 194–215. [\[CrossRef\]](#)
32. Fila, D.; Hubicki, Z.; Kolodynska, D. Recovery of metals from waste nickel-metal hydride batteries using multifunctional Diphonix resin. *Adsorpt. J. Int. Ads. Soc.* **2019**, *25*, 367–382. [\[CrossRef\]](#)
33. Zhang, W.; Ning, S.; Zhang, S.; Wang, S.; Zhou, J.; Wang, X.; Wei, Y. Synthesis of functional silica composite resin for the selective separation of zirconium from scandium. *Microporous Mesoporous Mater.* **2019**, *288*, 109602. [\[CrossRef\]](#)
34. Wu, S.; Wang, L.; Zhang, P.; El-Shall, H.; Moudgil, B.; Huang, X.; Zhao, L.; Zhang, L.; Feng, Z. Simultaneous recovery of rare earths and uranium from wet process phosphoric acid using solvent extraction with D2EHPA. *Hydrometallurgy* **2018**, *175*, 109–116. [\[CrossRef\]](#)
35. Hu, Y.; Florek, J.; Larivière, D.; Fontaine, F.G.; Kleitz, F. Recent advances in the separation of rare earth elements using mesoporous hybrid materials. *Chem. Rec.* **2018**, *18*, 1261–1276. [\[CrossRef\]](#)
36. Mondal, S.; Ghar, A.; Satpati, A.K.; Sinharoy, P.; Singh, D.K.; Sharma, J.N.; Sreenivas, T.; Kain, V. Recovery of rare earth elements from coal fly ash using TEHDGA impregnated resin. *Hydrometallurgy* **2019**, *185*, 93–101. [\[CrossRef\]](#)
37. Sun, X.; Ji, Y.; Chen, J.; Ma, J. Solvent impregnated resin prepared using task-specific ionic liquids for rare earth separation. *J. Rare Earths* **2009**, *27*, 932–936. [\[CrossRef\]](#)

38. Matsunaga, H.; Ismail, A.A.; Wakui, Y.; Yokoyama, T. Extraction of rare earth elements with 2-ethylhexyl hydrogen 2-ethylhexyl phosphonate impregnated resins having different morphology and reagent content. *React. Funct. Polym.* **2001**, *49*, 189–195. [\[CrossRef\]](#)
39. Page, M.J.; Soldenhoff, K.; Ogden, M.D. Comparative study of the application of chelating resins for rare earth recovery. *Hydrometallurgy* **2017**, *169*, 275–281. [\[CrossRef\]](#)
40. Selim, M.T.; Salem, S.S.; Mohamed, A.A.; El-Gamal, M.S.; Awad, M.F.; Fouda, A. Biological treatment of real textile effluent using *Aspergillus flavus* and *Fusarium oxysporium* and their consortium along with the evaluation of their phytotoxicity. *J. Fungi* **2021**, *7*, 193. [\[CrossRef\]](#)
41. Arrambide, C.; Arrachart, G.; Berthelon, S.; Wehbie, M.; Pellet-Rostaing, S. Extraction and recovery of rare earths by chelating phenolic copolymers bearing diglycolamic acid or diglycolamide moieties. *React. Funct. Polym.* **2019**, *142*, 147–158. [\[CrossRef\]](#)
42. Virolainen, S.; Repo, E.; Sainio, T. Recovering rare earth elements from phosphogypsum using a resin-in-leach process: Selection of resin, leaching agent, and eluent. *Hydrometallurgy* **2019**, *189*, 105125. [\[CrossRef\]](#)
43. Abdel-Rahman, A.A.H.; El-Aassy, I.E.E.; Fadia, Y.A.; Hamza, M.F. Studies on the uptake of rare earth elements on polyacrylamide-doxime resins from natural concentrate leachate solutions. *J. Dispersion Sci. Technol.* **2010**, *31*, 1128–1135. [\[CrossRef\]](#)
44. Hamza, M.F.; Abdel-Rahman, A.A.H.; Guibal, E. Magnetic glutamine-grafted polymer for the sorption of U(VI), Nd(III) and Dy(III). *J. Chem. Technol. Biotechnol.* **2018**, *93*, 1790–1806. [\[CrossRef\]](#)
45. Burakova, I.V.; Burakov, A.B.; Tkachev, A.G.; Troshkina, I.D.; Veselova, O.A.; Babkin, A.V.; Aung, W.M.; Ali, I. Kinetics of the adsorption of scandium and cerium ions in sulfuric acid solutions on a nanomodified activated carbon. *J. Mol. Liq.* **2018**, *253*, 277–283. [\[CrossRef\]](#)
46. Smith, Y.R.; Bhattacharyya, D.; Willhard, T.; Misra, M. Adsorption of aqueous rare earth elements using carbon black derived from recycled tires. *Chem. Eng. J.* **2016**, *296*, 102–111. [\[CrossRef\]](#)
47. Ashour, R.M.; Abdelhamid, H.N.; Abdel-Magied, A.F.; Abdel-Khalek, A.A.; Ali, M.M.; Uheida, A.; Muhammed, M.; Zou, X.; Dutta, J. Rare earth ions adsorption onto graphene oxide nanosheets. *Solvent Extr. Ion Exch.* **2017**, *35*, 91–103. [\[CrossRef\]](#)
48. Zhang, W.; Yu, S.Q.; Zhang, S.C.; Zhou, J.; Ning, S.Y.; Wang, X.P.; Wei, Y.Z. Separation of scandium from the other rare earth elements with a novel macro-porous silica-polymer based adsorbent HDEHP/SiO₂-P. *Hydrometallurgy* **2019**, *185*, 117–124. [\[CrossRef\]](#)
49. Ramasamy, D.L.; Puhakka, V.; Repo, E.; Sillanpää, M. Selective separation of scandium from iron, aluminium and gold rich wastewater using various amino and non-amino functionalized silica gels—A comparative study. *J. Clean. Prod.* **2018**, *170*, 890–901. [\[CrossRef\]](#)
50. Ramasamy, D.L.; Khan, S.; Repo, E.; Sillanpää, M. Synthesis of mesoporous and microporous amine and non-amine functionalized silica gels for the application of rare earth elements (REE) recovery from the waste water—understanding the role of pH, temperature, calcination and mechanism in Light REE and Heavy REE separation. *Chem. Eng. J.* **2017**, *322*, 56–65. [\[CrossRef\]](#)
51. Xiao, Y.; Huang, L.; Long, Z.; Feng, Z.; Wang, L. Adsorption ability of rare earth elements on clay minerals and its practical performance. *J. Rare Earths* **2016**, *34*, 543–548. [\[CrossRef\]](#)
52. Iannicelli-Zubiani, E.M.; Cristiani, C.; Dotelli, G.; Stampino, P.G.; Pelosato, R.; Mesto, E.; Schingaro, E.; Lacalamita, M. Use of natural clays as sorbent materials for rare earth ions: Materials characterization and set up of the operative parameters. *Waste Manag.* **2015**, *46*, 546–556. [\[CrossRef\]](#) [\[PubMed\]](#)
53. Li, Z.; Ning, S.; Zhu, H.; Wang, X.; Yin, X.; Fujita, T.; Wei, Y. Novel NbCo-MOF as an advanced peroxymonosulfate catalyst for organic pollutants removal: Growth, performance and mechanism study. *Chemosphere* **2022**, *288*, 132600. [\[CrossRef\]](#)
54. Roosen, J.; Binnemans, K. Adsorption and chromatographic separation of rare earths with EDTA- and DTPA-functionalized chitosan biopolymers. *J. Mater. Chem. A* **2014**, *2*, 1530–1540. [\[CrossRef\]](#)
55. Zheng, X.; Zhang, Y.; Bian, T.; Zhang, Y.; Zhang, F.; Yan, Y. Selective extraction of gadolinium using free-standing imprinted mesoporous carboxymethyl chitosan films with high capacity. *Cellulose* **2019**, *26*, 1209–1219. [\[CrossRef\]](#)
56. Gad, H.M.H.; Hamed, M.M.; Eldahab, H.; Moustafa, M.E.; El-Reefy, S.A. Radiation-induced grafting copolymerization of resin onto the surface of silica extracted from rice husk ash for adsorption of gadolinium. *J. Mol. Liq.* **2017**, *231*, 45–55. [\[CrossRef\]](#)
57. Rahman, M.L.; Sarjadi, M.S.; Arshad, S.E.; Yusoff, M.M.; Sarkar, S.M.; Musta, B. Kenaf cellulose-based poly(amidoxime) ligand for adsorption of rare earth ions. *Rare Met.* **2019**, *38*, 259–269. [\[CrossRef\]](#)
58. Wang, F.C.; Zhao, J.M.; Wei, X.T.; Huo, F.; Li, W.S.; Hu, Q.Y.; Liu, H.Z. Adsorption of rare earths(III) by calcium alginate-poly glutamic acid hybrid gels. *J. Chem. Technol. Biotechnol.* **2014**, *89*, 969–977. [\[CrossRef\]](#)
59. Abdel-Magied, A.F.; Abdelhamid, H.N.; Ashour, R.M.; Zou, X.; Forsberg, K. Hierarchical porous zeolitic imidazolate frameworks nanoparticles for efficient adsorption of rare-earth elements. *Microporous Mesoporous Mater.* **2019**, *278*, 175–184. [\[CrossRef\]](#)
60. HAMZA, M.F.; Abd Allh, M.; Guibal, E.; Adel, A.-H.; El Araby, R. Synthesis of a new pyrimidine-based sorbent for indium (III) removal from aqueous solutions—Application to ore leachate. *Sep. Purif. Technol.* **2023**, *314*, 123514. [\[CrossRef\]](#)
61. Zahra, M.H.; Hamza, M.F.; El-Habibi, G.; Abdel-Rahman, A.A.-H.; Mira, H.I.; Wei, Y.; Alotaibi, S.H.; Amer, H.H.; Goda, A.E.-S.; Hamad, N.A. Synthesis of a Novel Adsorbent Based on Chitosan Magnetite Nanoparticles for the High Sorption of Cr (VI) ions: A Study of Photocatalysis and Recovery on Tannery Effluents. *Catalysts* **2022**, *12*, 678. [\[CrossRef\]](#)
62. Ravi, S.; Lee, Y.-R.; Yu, K.; Ahn, J.-W.; Ahn, W.-S. Benzene triamido-tetraphosphonic acid immobilized on mesoporous silica for adsorption of Nd³⁺ ions in aqueous solution. *Microporous Mesoporous Mater.* **2018**, *258*, 62–71. [\[CrossRef\]](#)

63. Maranescu, B.; Lupa, L.; Visa, A. Synthesis, characterization and rare earth elements adsorption properties of phosphonate metal organic frameworks. *Appl. Surf. Sci.* **2019**, *481*, 83–91. [\[CrossRef\]](#)
64. Tang, R.; Zhang, Y.; Zhang, Y.; Yu, Z. Synthesis and characterization of chitosan based dye containing quaternary ammonium group. *Carbohydr. Polym.* **2016**, *139*, 191–196. [\[CrossRef\]](#)
65. Xu, J.; Lian, J.; You, L.; Zhao, Z. Characteristics and properties of the quaternary ammonium-functionalized micron chitosan modified by zinc citrate chelates for encapsulation of betanin. *Colloids Surf. B Biointerfaces* **2022**, *218*, 112752. [\[CrossRef\]](#)
66. Xu, J.; Lai, H.; You, L.; Zhao, Z. Improvement of the stability and anti-AGEs ability of betanin through its encapsulation by chitosan-TPP coated quaternary ammonium-functionalized mesoporous silica nanoparticles. *Int. J. Biol. Macromol.* **2022**, *222*, 1388–1399. [\[CrossRef\]](#)
67. Hamza, M.F.; Lu, S.; Salih, K.A.; Mira, H.; Dhmees, A.S.; Fujita, T.; Wei, Y.; Vincent, T.; Guibal, E. As (V) sorption from aqueous solutions using quaternized algal/polyethyleneimine composite beads. *Sci. Total Environ.* **2020**, *719*, 137396. [\[CrossRef\]](#) [\[PubMed\]](#)
68. Hamza, M.F.; Guibal, E.; Althumayri, K.; Wei, Y.; Eid, A.M.; Fouda, A. Poly-condensation of N-(2-acetamido)-2-aminoethanesulfonic acid with formaldehyde for the synthesis of a highly efficient sorbent for Cs (I). *Chem. Eng. J.* **2022**, *454*, 140155. [\[CrossRef\]](#)
69. Hamza, M.F.; Guibal, E.; Abdel-Rahman, A.A.-H.; Salem, M.; Khalafalla, M.S.; Wei, Y.; Yin, X. Enhancement of Cerium Sorption onto Urea-Functionalized Magnetite Chitosan Microparticles by Sorbent Sulfonation—Application to Ore Leachate. *Molecules* **2022**, *27*, 7562. [\[CrossRef\]](#)
70. Fouda, A.; Hamza, M.F.; Shaheen, T.I.; Wei, Y. Nanotechnology and smart textiles: Sustainable developments of applications. *Front. Bioeng. Biotechnol.* **2022**, *10*, 1002887. [\[CrossRef\]](#) [\[PubMed\]](#)
71. Gamzazade, A.; Sklyar, A.; Nasibov, S.; Sushkov, I.; Shashkov, A.; Knirel, Y. Structural features of sulfated chitosans. *Carbohydr. Polym.* **1997**, *34*, 113–116. [\[CrossRef\]](#)
72. Varma, A.J.; Deshpande, S.V.; Kennedy, J.F. Metal complexation by chitosan and its derivatives: A review. *Carbohydr. Polym.* **2004**, *55*, 77–93. [\[CrossRef\]](#)
73. Kyzas, G.Z.; Siafaka, P.I.; Pavlidou, E.G.; Chrissafis, K.J.; Bikiaris, D.N. Synthesis and adsorption application of succinyl-grafted chitosan for the simultaneous removal of zinc and cationic dye from binary hazardous mixtures. *Chem. Eng. J.* **2015**, *259*, 438–448. [\[CrossRef\]](#)
74. Borsagli, F.; Mansur, A.A.P.; Chagas, P.; Oliveira, L.C.A.; Mansur, H.S. O-carboxymethyl functionalization of chitosan: Complexation and adsorption of Cd (II) and Cr (VI) as heavy metal pollutant ions. *React. Funct. Polym.* **2015**, *97*, 37–47. [\[CrossRef\]](#)
75. Juang, R.S.; Ju, C.Y. Equilibrium sorption of copper(II)-ethylenediaminetetraacetic acid chelates onto cross-linked, polyaminated chitosan beads. *Ind. Eng. Chem. Res.* **1997**, *36*, 5403–5409. [\[CrossRef\]](#)
76. Dragan, E.S.; Humelnicu, D.; Dinu, M.V. Development of chitosan-poly(ethyleneimine) based double network cryogels and their application as superadsorbents for phosphate. *Carbohydr. Polym.* **2019**, *210*, 17–25. [\[CrossRef\]](#) [\[PubMed\]](#)
77. Elsalamouny, A.R.; Desouky, O.A.; Mohamed, S.A.; Galhoum, A.A.; Guibal, E. Uranium and neodymium biosorption using novel chelating polysaccharide. *Int. J. Biol. Macromol.* **2017**, *104*, 963–968. [\[CrossRef\]](#)
78. Maranescu, B.; Popa, A.; Lupa, L.; Maranescu, V.; Visa, A. Use of chitosan complex with aminophosphonic groups and cobalt for the removal of Sr²⁺ ions. *Sep. Sci. Technol.* **2018**, *53*, 1058–1064. [\[CrossRef\]](#)
79. Ramos, V.M.; Rodriguez, N.M.; Diaz, M.F.; Rodriguez, M.S.; Heras, A.; Agullo, E. N-methylene phosphonic chitosan. Effect of preparation methods on its properties. *Carbohydr. Polym.* **2003**, *52*, 39–46. [\[CrossRef\]](#)
80. Zhang, S.; Zhang, Y.; Ding, J.; Zhang, Z.; Gao, C.; Halimi, M.; Demey, H.; Yang, Z.; Yang, W. High phosphate removal using La (OH) 3 loaded chitosan based composites and mechanistic study. *J. Environ. Sci.* **2021**, *106*, 105–115. [\[CrossRef\]](#)
81. Hamza, M.F.; Abu Khoziem, H.A.; Khalafalla, M.S.; Abdellah, W.M.; Zaki, D.I.; Althumayri, K.; Wei, Y. Ecofriendly Composite as a Promising Material for Highly-Performance Uranium Recovery from Different Solutions. *Toxics* **2022**, *10*, 490. [\[CrossRef\]](#)
82. Hamza, M.F.; Wei, Y.; Althumayri, K.; Fouda, A.; Hamad, N.A. Synthesis and Characterization of Functionalized Chitosan Nanoparticles with Pyrimidine Derivative for Enhancing Ion Sorption and Application for Removal of Contaminants. *Materials* **2022**, *15*, 4676. [\[CrossRef\]](#)
83. Hamza, M.F.; Salih, K.A.; Zhou, K.; Wei, Y.; Khoziem, H.A.A.; Alotaibi, S.H.; Guibal, E. Effect of bi-functionalization of algal/polyethyleneimine composite beads on the enhancement of tungstate sorption: Application to metal recovery from ore leachate. *Sep. Purif. Technol.* **2022**, *290*, 120893. [\[CrossRef\]](#)
84. Fouda, A.; Hassan, S.E.-D.; Eid, A.M.; Abdel-Rahman, M.A.; Hamza, M.F. Light enhanced the antimicrobial, anticancer, and catalytic activities of selenium nanoparticles fabricated by endophytic fungal strain, *Penicillium crustosum* EP-1. *Sci. Rep.* **2022**, *12*, 11834. [\[CrossRef\]](#)
85. Amin, M.A.; Ismail, M.A.; Badawy, A.A.; Awad, M.A.; Hamza, M.F.; Awad, M.F.; Fouda, A. The Potency of fungal-fabricated selenium nanoparticles to improve the growth performance of *Helianthus annuus* L. and control of cutworm *Agrotis ipsilon*. *Catalysts* **2021**, *11*, 1551. [\[CrossRef\]](#)
86. Fouda, A.; Awad, M.A.; Eid, A.M.; Saied, E.; Barghoth, M.G.; Hamza, M.F.; Awad, M.F.; Abdelbary, S.; Hassan, S.E.-D. An eco-friendly approach to the control of pathogenic microbes and *Anopheles stephensi* malarial vector using magnesium oxide nanoparticles (Mg-nps) fabricated by *Penicillium chrysogenum*. *Int. J. Mol. Sci.* **2021**, *22*, 5096. [\[CrossRef\]](#) [\[PubMed\]](#)
87. Hamza, M.F.; Abdel-Rahman, A.A.-H.; Negm, A.S.; Hamad, D.M.; Khalafalla, M.S.; Fouda, A.; Wei, Y.; Amer, H.H.; Alotaibi, S.H.; Goda, A.E.-S. Grafting of Thiazole Derivative on Chitosan Magnetite Nanoparticles for Cadmium Removal—Application for Groundwater Treatment. *Polymers* **2022**, *14*, 1240. [\[CrossRef\]](#) [\[PubMed\]](#)

88. Pearson, R.G. Acids and bases. *Science* **1966**, *151*, 172–177. [[CrossRef](#)] [[PubMed](#)]
89. Rafik, B.; Nouredine, O.; Abderabbou, A.; Habib, L. Self-diffusion coefficients of the trivalent f-element ion series in dilute and moderately dilute aqueous solutions: A comparative study between europium, gadolinium, terbium and berkelium. In *IOP Conference Series-Materials Science and Engineering*; Rao, L., Tobin, J.G., Shuh, D.K., Eds.; IOP Publishing: Bristol, UK, 2010; Volume 9.
90. Yang, Y.J.; Alexandratos, S.D. Affinity of polymer-supported reagents for lanthanides as a function of donor atom polarizability. *Ind. Eng. Chem. Res.* **2009**, *48*, 6173–6187. [[CrossRef](#)]
91. Zhang, P.; Wang, Y.; Zhang, D.; Bai, H.; Tarasov, V.V. Calixarene-functionalized graphene oxide composites for adsorption of neodymium ions from the aqueous phase. *RSC Adv.* **2016**, *6*, 30384–30394. [[CrossRef](#)]
92. Hisada, M.; Kawase, Y. Recovery of rare-earth metal neodymium from aqueous solutions by poly-gamma-glutamic acid and its sodium salt as biosorbents: Effects of solution pH on neodymium recovery mechanisms. *J. Rare Earths* **2018**, *36*, 528–536. [[CrossRef](#)]
93. Wang, F.; Zhao, J.; Liu, H.; Luo, Y.; Wang, W. Preparation of double carboxylic corn stalk gels and their adsorption properties towards rare earths(III). *Waste Biomass Valorization* **2018**, *9*, 1945–1954. [[CrossRef](#)]
94. Krishna, P.G.; Gladis, J.M.; Rao, T.P.; Naidu, G.R. Selective recognition of neodymium(III) using ion imprinted polymer particles. *J. Mol. Recognit.* **2005**, *18*, 109–116. [[CrossRef](#)]
95. Oliveira, R.C.; Garcia, O., Jr. Study of biosorption of rare earth metals (La, Nd, Eu, Gd) by *Sargassum* sp. biomass in batch systems: Physicochemical evaluation of kinetics and adsorption models. In *Biorecovery: A Meeting Point between Microbial Ecology, Metal Recovery Processes and Environmental Remediation*; Donati, E.R., Viera, M.R., Tavani, E.L., Giaveno, M.A., Lavalle, T.L., Chiacchiarini, P.A., Eds.; Advanced Materials Research; Trans Tech Publications: Stafa-Zurich, Switzerland, 2009; Volume 71–73, pp. 605–608.
96. Vlachou, A.; Symeopoulos, B.D.; Koutinas, A.A. A comparative study of neodymium sorption by yeast cells. *Radiochim. Acta* **2009**, *97*, 437–441. [[CrossRef](#)]
97. Park, H.-J.; Tavlarides, L.L. Adsorption of neodymium(III) from aqueous solutions using a phosphorus functionalized adsorbent. *Ind. Eng. Chem. Res.* **2010**, *49*, 12567–12575. [[CrossRef](#)]
98. Zhang, L.; Wu, D.; Zhu, B.; Yang, Y.; Wang, L. Adsorption and selective separation of neodymium with magnetic alginate microcapsules containing the extractant 2-ethylhexyl phosphonic acid mono-2-ethylhexyl ester. *J. Chem. Eng. Data* **2011**, *56*, 2280–2289. [[CrossRef](#)]
99. Ashour, R.M.; El-Sayed, R.; Abdel-Magied, A.F.; Abdel-Khalek, A.A.; Ali, M.M.; Forsberg, K.; Uheida, A.; Muhammed, M.; Dutta, J. Selective separation of rare earth ions from aqueous solution using functionalized magnetite nanoparticles: Kinetic and thermodynamic studies. *Chem. Eng. J.* **2017**, *327*, 286–296. [[CrossRef](#)]
100. Mohamed, W.R.; Metwally, S.S.; Ibrahim, H.A.; El-Sherief, E.A.; Mekhamer, H.S.; Moustafa, I.M.I.; Mabrouk, E.M. Impregnation of task-specific ionic liquid into a solid support for removal of neodymium and gadolinium ions from aqueous solution. *J. Mol. Liq.* **2017**, *236*, 9–17. [[CrossRef](#)]
101. Elsalamouny, A.R.; Desouky, O.A.; Mohamed, S.A.; Galhoum, A.A.; Guibal, E. Evaluation of adsorption behavior for U(VI) and Nd(III) ions onto fumarated polystyrene microspheres. *J. Radioanal. Nucl. Chem.* **2017**, *314*, 429–437. [[CrossRef](#)]
102. Kucuker, M.A.; Wiecek, N.; Kuchta, K.; Copt, N.K. Biosorption of neodymium on *Chlorella vulgaris* in aqueous solution obtained from hard disk drive magnets. *PLoS ONE* **2017**, *12*, e0175255. [[CrossRef](#)]
103. Liao, Q.; Zou, D.; Pan, W.; Linghu, W.; Shen, R.; Li, X.; Asiri, A.M.; Alamry, K.A.; Sheng, G.; Zhan, L.; et al. Highly efficient capture of Eu(III), La(III), Nd(III), Th(IV) from aqueous solutions using g-C₃N₄ nanosheets. *J. Mol. Liq.* **2018**, *252*, 351–361. [[CrossRef](#)]
104. Hamadneh, I.; Alatawi, A.; Zalloum, R.; Albuqain, R.; Alsotari, S.; Khalili, F.I.; Al-Dujaili, A.H. Comparison of Jordanian and standard diatomaceous earth as an adsorbent for removal of Sm(III) and Nd(III) from aqueous solution. *Environ. Sci. Pollut. Res.* **2019**, *26*, 20969–20980. [[CrossRef](#)]
105. Najafi, M.; Chevinli, A.S.; Srivastava, V.; Sillanpaa, M. Augmentation of neodymium ions removal from water using two lanthanides-based MOF: Ameliorated efficiency by synergistic interaction of two lanthanides. *J. Chem. Eng. Data* **2019**, *64*, 3105–3112. [[CrossRef](#)]
106. Salih, K.A.M.; Hamza, M.F.; Mira, H.; Wei, Y.; Gao, F.; Atta, A.M.; Fujita, T.; Guibal, E. Nd(III) and Gd(III) sorption on mesoporous amine-functionalized polymer/SiO₂ composite. *Molecules* **2021**, *26*, 1049. [[CrossRef](#)] [[PubMed](#)]
107. Lopez-Ramon, M.V.; Stoeckli, F.; Moreno-Castilla, C.; Carrasco-Marin, F. On the characterization of acidic and basic surface sites on carbons by various techniques. *Carbon* **2009**, *37*, 1215–1221. [[CrossRef](#)]
108. Nayak, A.K.; Pal, A. Development and validation of an adsorption kinetic model at solid-liquid interface using normalized Gudermannian function. *J. Mol. Liq.* **2019**, *276*, 67–77. [[CrossRef](#)]
109. Hamza, M.F.; El Aassy, I.E.; Ahmed, F.Y.; Abdel-Rahman, A.A.-H.; Atta, A.M. Separation of uranium and rare earth elements with high purity from low-grade gibbsite-bearing shale ore by different chelating resins. *J. Dispers. Sci. Technol.* **2012**, *33*, 482–489. [[CrossRef](#)]
110. Fouda, A.; Salem, S.S.; Wassel, A.R.; Hamza, M.F.; Shaheen, T.I. Optimization of green biosynthesized visible light active CuO/ZnO nano-photocatalysts for the degradation of organic methylene blue dye. *Heliyon* **2020**, *6*, e04896. [[CrossRef](#)] [[PubMed](#)]
111. Zhang, H.; Li, C.; Chen, X.; Fu, H.; Chen, Y.; Ning, S.; Fujita, T.; Wei, Y.; Wang, X. Layered ammonium vanadate nanobelt as efficient adsorbents for removal of Sr²⁺ and Cs⁺ from contaminated water. *J. Colloid Interface Sci.* **2022**, *615*, 110–123. [[CrossRef](#)]

112. Fouda, A.; Eid, A.M.; Guibal, E.; Hamza, M.F.; Hassan, S.E.-D.; Alkhalifah, D.H.M.; El-Hossary, D. Green Synthesis of Gold Nanoparticles by Aqueous Extract of Zingiber officinale: Characterization and Insight into Antimicrobial, Antioxidant, and In Vitro Cytotoxic Activities. *Appl. Sci.* **2022**, *12*, 12879. [\[CrossRef\]](#)
113. Chen, Y.; Ning, S.; Zhong, Y.; Li, Z.; Wang, J.; Chen, L.; Yin, X.; Fujita, T.; Wei, Y. Study on highly efficient separation of zirconium from scandium with TODGA-modified macroporous silica-polymer based resin. *Sep. Purif. Technol.* **2023**, *305*, 122499. [\[CrossRef\]](#)
114. Hamza, M.F.; Salih, K.A.; Adel, A.-H.; Zayed, Y.E.; Wei, Y.; Liang, J.; Guibal, E. Sulfonic-functionalized algal/PEI beads for scandium, cerium and holmium sorption from aqueous solutions (synthetic and industrial samples). *Chem. Eng. J.* **2021**, *403*, 126399. [\[CrossRef\]](#)
115. Hamza, M.F.; Guibal, E.; Althumayri, K.; Vincent, T.; Yin, X.; Wei, Y.; Li, W. New Process for the Sulfonation of Algal/PEI Biosorbent for Enhancing Sr (II) Removal from Aqueous Solutions—Application to Seawater. *Molecules* **2022**, *27*, 7128. [\[CrossRef\]](#)
116. Hamza, M.F.; Adel, A.-H.; Hawata, M.A.; El Araby, R.; Guibal, E.; Fouda, A.; Wei, Y.; Hamad, N.A. Functionalization of magnetic chitosan microparticles—Comparison of trione and trithione grafting for enhanced silver sorption and application to metal recovery from waste X-ray photographic films. *J. Environ. Chem. Eng.* **2022**, *10*, 107939. [\[CrossRef\]](#)
117. Fouda, A.; Awad, M.A.; AL-Faifi, Z.E.; Gad, M.E.; Al-Khalaf, A.A.; Yahya, R.; Hamza, M.F. Aspergillus flavus-Mediated Green Synthesis of Silver Nanoparticles and Evaluation of Their Antibacterial, Anti-Candida, Acaricides, and Photocatalytic Activities. *Catalysts* **2022**, *12*, 462. [\[CrossRef\]](#)
118. Fouda, A.; Eid, A.M.; Abdel-Rahman, M.A.; El-Belely, E.F.; Awad, M.A.; Hassan, S.E.-D.; Al-Faifi, Z.E.; Hamza, M.F. Enhanced antimicrobial, cytotoxicity, larvicidal, and repellence activities of brown algae, cystoseira crinita-mediated green synthesis of magnesium oxide nanoparticles. *Front. Bioeng. Biotechnol.* **2022**, *10*, 849921. [\[CrossRef\]](#) [\[PubMed\]](#)
119. Fouda, A.; Hassan, S.E.-D.; Eid, A.M.; Awad, M.A.; Althumayri, K.; Badr, N.F.; Hamza, M.F. Endophytic bacterial strain, Brevibacillus brevis-mediated green synthesis of copper oxide nanoparticles, characterization, antifungal, in vitro cytotoxicity, and larvicidal activity. *Green Process. Synth.* **2022**, *11*, 931–950. [\[CrossRef\]](#)
120. Hamza, M.F.; Mira, H.; Wei, Y.; Aboelenin, S.M.; Guibal, E.; Salem, W.M. Sulfonation of chitosan for enhanced sorption of Li (I) from acidic solutions—Application to metal recovery from waste Li-ion mobile battery. *Chem. Eng. J.* **2022**, *441*, 135941. [\[CrossRef\]](#)
121. Hamza, M.F.; Wei, Y.; Khalafalla, M.S.; Abed, N.S.; Fouda, A.; Elwakeel, K.Z.; Guibal, E.; Hamad, N.A. U (VI) and Th (IV) recovery using silica beads functionalized with urea-or thiourea-based polymers—Application to ore leachate. *Sci. Total Environ.* **2022**, *821*, 153184. [\[CrossRef\]](#) [\[PubMed\]](#)
122. Hamza, M.F.; Goda, A.E.-S.; Ning, S.; Mira, H.I.; Abdel-Rahman, A.A.-H.; Wei, Y.; Fujita, T.; Amer, H.H.; Alotaibi, S.H.; Fouda, A. Photocatalytic Efficacy of Heterocyclic Base Grafted Chitosan Magnetite Nanoparticles on Sorption of Pb (II); Application on Mining Effluent. *Catalysts* **2022**, *12*, 330. [\[CrossRef\]](#)
123. Hamza, M.F.; Alotaibi, S.H.; Wei, Y.; Mashaal, N.M. High-Performance Hydrogel Based on Modified Chitosan for Removal of Heavy Metal Ions in Borehole: A Case Study from the Bahariya Oasis, Egypt. *Catalysts* **2022**, *12*, 721. [\[CrossRef\]](#)
124. Fouda, A.; Hassan, S.E.-D.; Saied, E.; Hamza, M.F. Photocatalytic degradation of real textile and tannery effluent using biosynthesized magnesium oxide nanoparticles (MgO-NPs), heavy metal adsorption, phytotoxicity, and antimicrobial activity. *J. Environ. Chem. Eng.* **2021**, *9*, 105346. [\[CrossRef\]](#)
125. Hamza, M.F.; Wei, Y.; Guibal, E. Quaternization of algal/PEI beads (a new sorbent): Characterization and application to scandium sorption from aqueous solutions. *Chem. Eng. J.* **2020**, *383*, 123210. [\[CrossRef\]](#)
126. Lin-Vien, D.; Colthup, N.B.; Fateley, W.G.; Grasselli, J.G. CHAPTER 16—Organophosphorus Compounds. In *The Handbook of Infrared and Raman Characteristic Frequencies of Organic Molecules*; Lin-Vien, D., Colthup, N.B., Fateley, W.G., Grasselli, J.G., Eds.; Academic Press: San Diego, CA, USA, 1991; pp. 263–276.
127. Coates, J. Interpretation of Infrared Spectra, A Practical Approach. In *Encyclopedia of Analytical Chemistry*; John Wiley & Sons, Ltd.: Hoboken, NJ, USA, 2006; pp. 1–23.
128. Hamza, M.F.; Hamad, N.A.; Hamad, D.M.; Khalafalla, M.S.; Abdel-Rahman, A.A.-H.; Zeid, I.F.; Wei, Y.; Hessien, M.M.; Fouda, A.; Salem, W.M. Synthesis of eco-friendly biopolymer, alginate-chitosan composite to adsorb the heavy metals, Cd (II) and Pb (II) from contaminated effluents. *Materials* **2021**, *14*, 2189. [\[CrossRef\]](#)
129. Hamza, M.F.; Mubark, A.E.; Wei, Y.; Vincent, T.; Guibal, E. Quaternization of composite algal/PEI beads for enhanced uranium sorption—Application to ore acidic leachate. *Gels* **2020**, *6*, 12. [\[CrossRef\]](#)
130. Hamza, M.F.; Fouda, A.; Wei, Y.; El Aassy, I.E.; Alotaibi, S.H.; Guibal, E.; Mashaal, N.M. Functionalized biobased composite for metal decontamination—Insight on uranium and application to water samples collected from wells in mining areas (Sinai, Egypt). *Chem. Eng. J.* **2022**, *431*, 133967. [\[CrossRef\]](#)
131. Hamza, M.F.; Sallam, O.R.; Khalafalla, M.S.; Abbas, A.E.A.; Wei, Y. Geological and radioactivity studies accompanied by uranium recovery: Um Bogma Formation, southwestern Sinai, Egypt. *J. Radioanal. Nucl. Chem.* **2020**, *324*, 1039–1051. [\[CrossRef\]](#)
132. Hamza, M.F. Grafting of quaternary ammonium groups for uranium (VI) recovery: Application on natural acidic leaching liquor. *J. Radioanal. Nucl. Chem.* **2019**, *322*, 519–532. [\[CrossRef\]](#)
133. Tien, C. *Adsorption Calculations and Modeling*; Butterworth-Heinemann: Newton, MA, USA, 1994; p. 243.
134. Lima, É.C.; Dehghani, M.H.; Guleria, A.; Sher, F.; Karri, R.R.; Dotto, G.L.; Tran, H.N. CHAPTER 3—Adsorption: Fundamental aspects and applications of adsorption for effluent treatment. In *Green Technologies for the Defluoridation of Water*; Hadi Dehghani, M., Karri, R., Lima, E., Eds.; Elsevier: Amsterdam, The Netherlands, 2021; pp. 41–88.

135. Buema, G.; Lupu, N.; Chiriac, H.; Ciobanu, G.; Bucur, R.D.; Bucur, D.; Favier, L.; Harja, M. Performance assessment of five adsorbents based on fly ash for removal of cadmium ions. *J. Mol. Liq.* **2021**, *333*, 115932. [[CrossRef](#)]
136. Crank, J. *The Mathematics of Diffusion*, 2nd ed.; Oxford University Press: Oxford, UK, 1975; p. 414.
137. Ho, Y.S.; McKay, G. Pseudo-second order model for sorption processes. *Process. Biochem.* **1999**, *34*, 451–465. [[CrossRef](#)]

Disclaimer/Publisher’s Note: The statements, opinions and data contained in all publications are solely those of the individual author(s) and contributor(s) and not of MDPI and/or the editor(s). MDPI and/or the editor(s) disclaim responsibility for any injury to people or property resulting from any ideas, methods, instructions or products referred to in the content.